GDR HydroGEMM

Hydrogen storage in salt caverns: evolution of salt permeability and hydromechanical modelling at the cavern scale under cycling conditions.

Dennys Coarita, **Fabrice Golfier**, Dragan Grgic, Farah Al Sahyouni, Mountaka Souley, Long Cheng

Université de Lorraine, CNRS, UMR 7359 GeoRessources, Nancy (France)

Institut National de l'Environnement Industriel et des Risques (Ineris), Nancy, France

Funding : ROSTOCK-H Geodénergies project, Grand Est Region Council, Carnot ICEEL

GENERAL CONTEXT: energy transition and H_2 storage

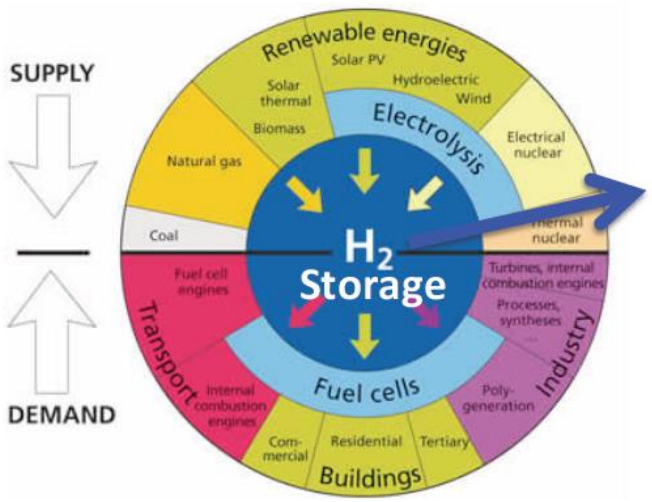

Hydrogen: versatile and promising carrier for energy transition

Currently produced from fossil fuels but from renewable energies in the future (green hydrogen)

Clean hydrogen (green and/or blue) should play a key role in the world transition to achieve carbon neutrality before 2050

- ✓ large-scale electricity storage
- ✓ decarbonize uses that are difficult to electrify
- ✓ use in industrial processes

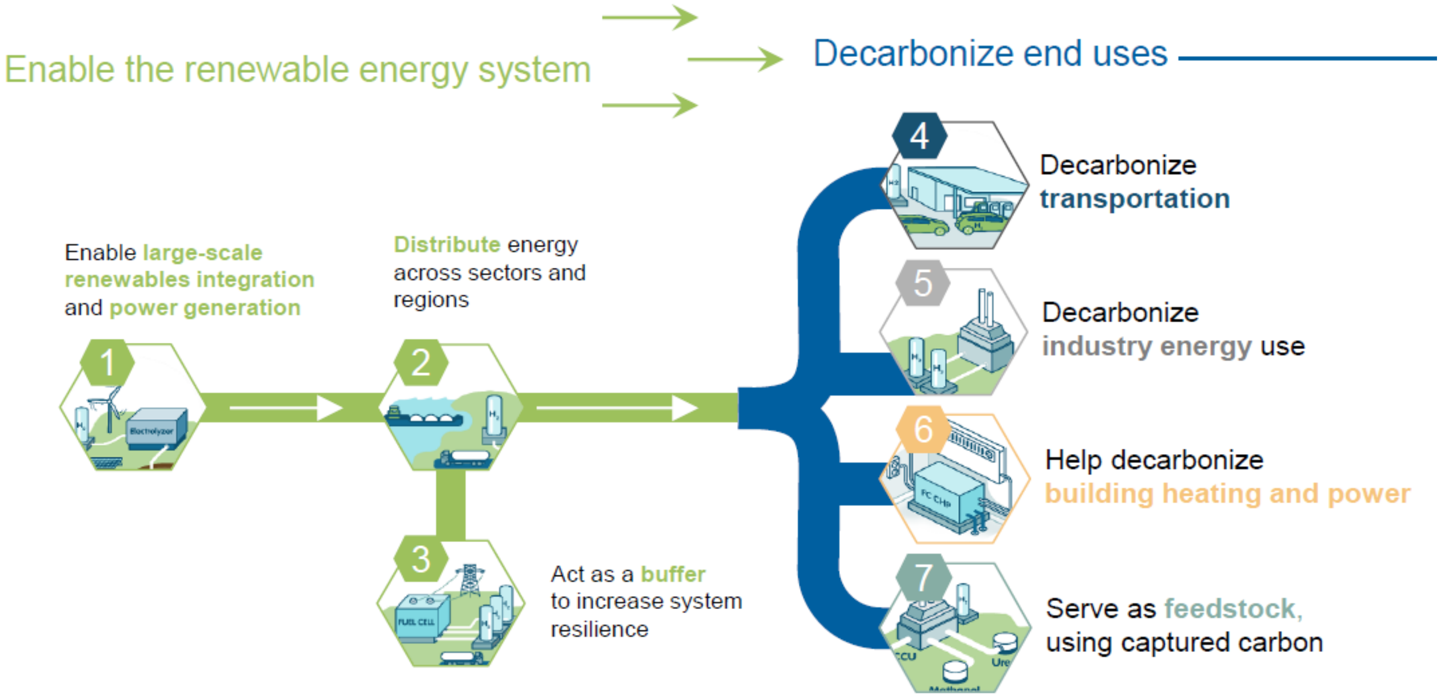

GENERAL CONTEXT: massive H_2 storage

Storing hydrogen in large quantities is the best option

Massive Storage ➡ Underground storage

2 solutions

Storage in deep aquifers

Storage in salt caverns

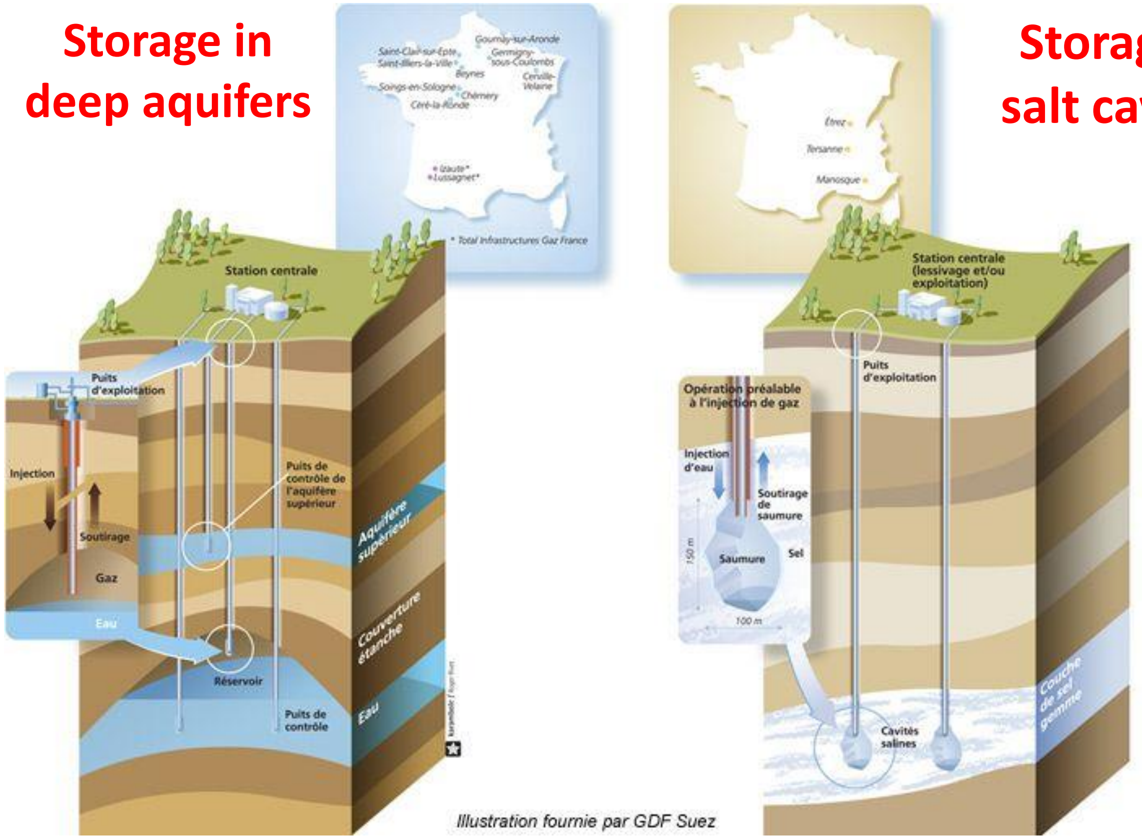

Illustration fournie par GDF Suez

Storage in salt cavern

Most secure and economical solution for large volumes of H_2

Only 4 salt caverns in operation worldwide (e.g., Spindletop USA, Teeside UK…)

but many industrial pilot sites in preparation worldwide (e.g., Etrez, France)

PROBLEM

Specific constraints compared to conventional gas storage

- High danger and mobility of H_2 (low density and viscosity, high diffusion)
- Need to accurately predict the extent of potential leaks of H_2 to ensure safe storage: **sealing of salt?**

Strong temperature (0-50 °C) and gas pressure (2-6 MPa for a 350 m deep cavern) variations in the salt cavern depending on the injection-production cycles (depends on usage)

→ Thermo-mechanical damage of rock salt in the near field (close to the wall) → permeability ↗

FOCUS OF THE STUDY

Characterize the ThermoHydroMechanical behaviour of rock salt

- Mechanical properties of initial material
- Impact of damage processes on rock salt permeability
- Viscoplasticity effect (self-healing process)
- Impact of mechanical (static and dynamic) and thermal (dynamic) fatigue

Grgic, D., Al Sahyouni, F., Golfier, F. Moumni, M. & Schoumacker, L., 2022. Evolution of gas permeability of rock salt under different loading conditions and implications on the underground hydrogen storage in salt caverns. *Rock Mechanics and Rock Engineering, 55(1):1-24.*

MATERIALS AND METHODS

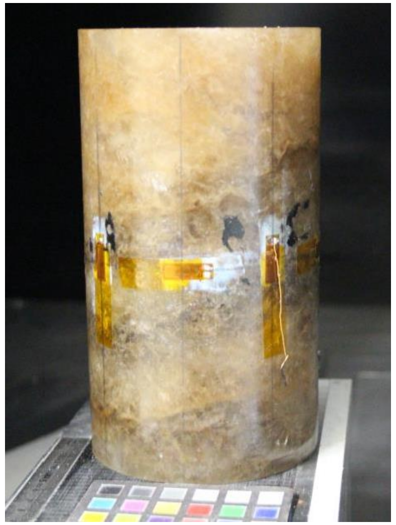

Cylindrical sample of rock salt (ϕ = 100 mm; H = 200 mm)

Rock salt samples

- Salt bed of the Alsace potash mines (530 m depth) in the East region of France (Stocamine site for ultimate waste storage)
- Sannoisian-Oligocene (Cenozoic) geological stage
- Considered as a natural analogue of salt caverns used for in-situ H_2 storage
- Very low initial porosity (~ 1%) composed mainly of infrapores (nanometric size) that connect dispersed cracks and macropores

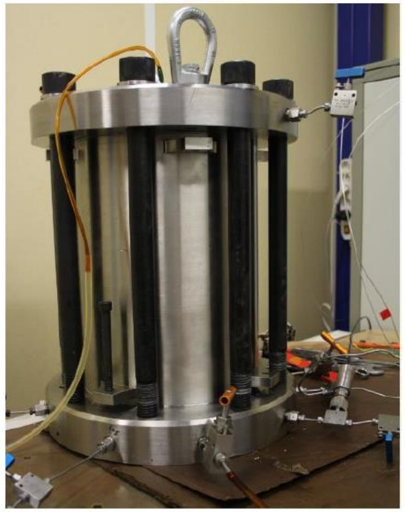

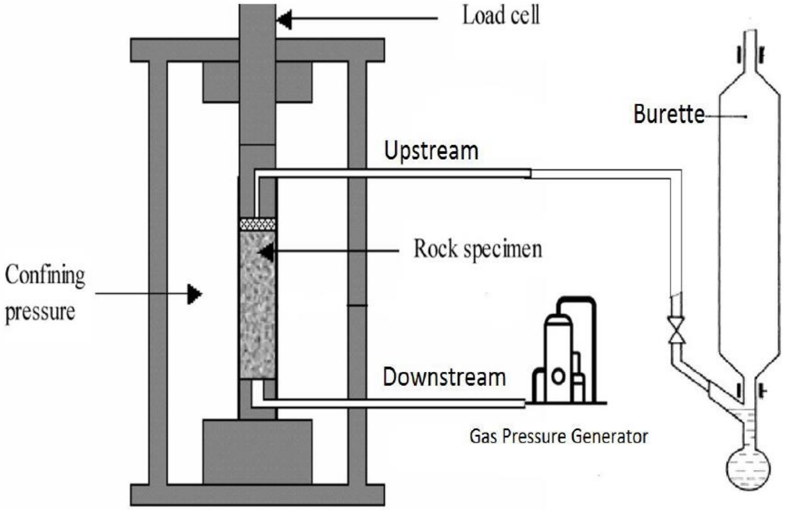

Experimental device

Experimental device

- Large scale triaxial compression cell
- Continuous measurement of deformations (strain gages)
- Continuous measurement of gas (He) permeability with the steady-state method
- Pressures controlled with precision syringe pumps

EXPERIMENTAL PROGRAM

Characterisation of the mechanical behaviour

- Hydrostatic compression tests
- Uniaxial and triaxial compression tests

→ Characterization of short-term deformation mechanisms (plasticity, micro-cracking damage)

Gas permeability measurements

- Under hydrostatic loading and triaxial loading with different confining pressures

→ Analyse the impact of the deformation mechanisms on permeability

- At different gas pressures

→ Analyse the slippage (Klinkenberg) effect and obtain the intrinsic gas permeability

- Under dynamic (cyclic) and static (creep test) triaxial loading, and under dynamic thermal loading

→ Analyse the impact of mechanical and thermal fatigue

MECHANICAL BEHAVIOUR OF ROCK SALT

Under hydrostatic loading

- **Isotropic** mechanical behaviour
- The behaviour is **elastic** (irreversible) and linear up to 30 MPa

→ No large initial cracks

- No poromechanical coupling (Biot's coefficient ~ 0)

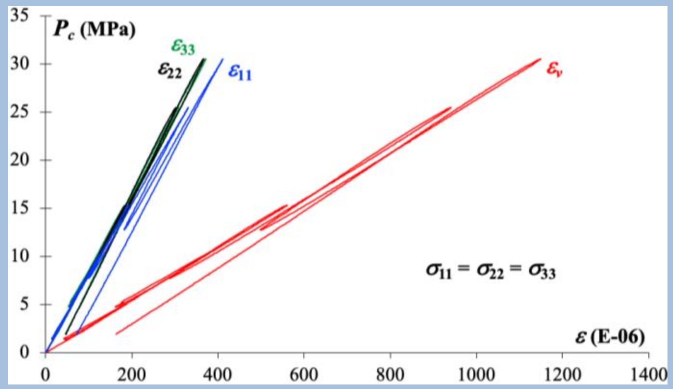

Stress-strain curves of an hydrostatic compression test

Under deviatoric loading

- **Very low elastic limit** (yield strength)
- **Crack initiation and dilatancy thresholds increase** with the confining pressure (Pc)
- **Dilatant and irreversible microcracking damage** develops at low Pc (0 and 1 MPa)
- Behaviour becomes **fully plastic** (ductile) at high Pc (5 MPa)

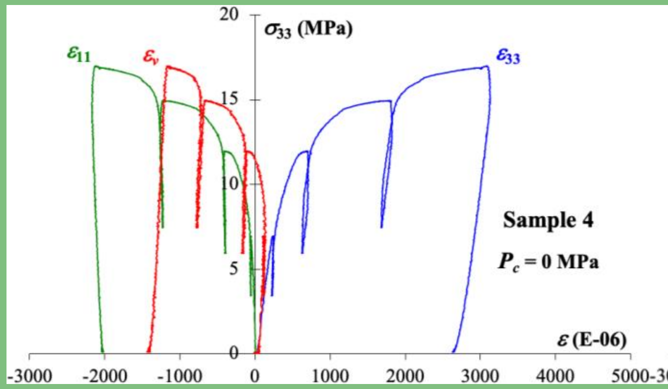

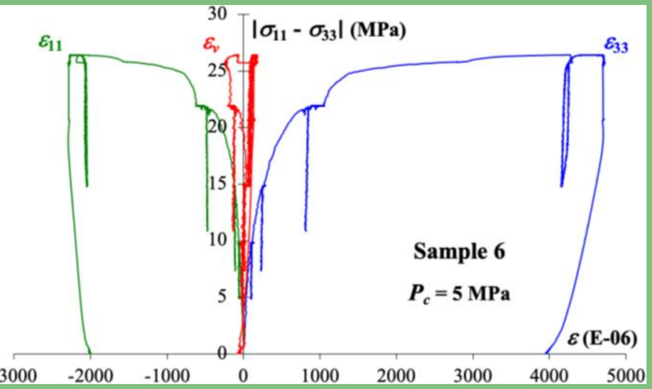

Stress-strain curves of of uniaxial (left) and triaxial (right) compression tests

- Dilatancy threshold ⟷ important increase of permeability due to cumulated microcracking damage

INTRINSIC PERMEABILITY OF ROCK SALT

Klinkenberg (slippage) effect

- **Klinkenberg effect** (i.e., decrease of permeability with the increase in gas pressure) only observed for the less permeable (and then less initially damaged) samples
- When it appears, the gas flow falls in **transitional regime** in weakly damaged rock salt

Evolution of apparent permeability k_a as a function of mean gas pressure at different deviatoric stress levels during triaxial compression tests

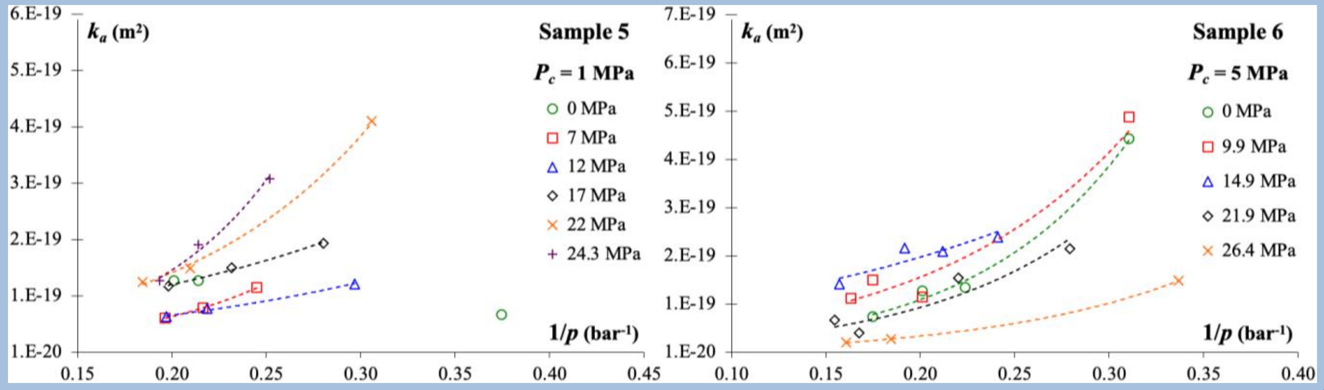

Initial permeability

- The initial intrinsic permeability of the studied rock salt ranges over more than 4 orders of magnitude: 10^{-16} to 5×10^{-21} m²
- Wide permeability range of the as-received samples due to the presence of cracks caused by the stress relaxation (induced by core drilling or cavity excavation) and sample preparation

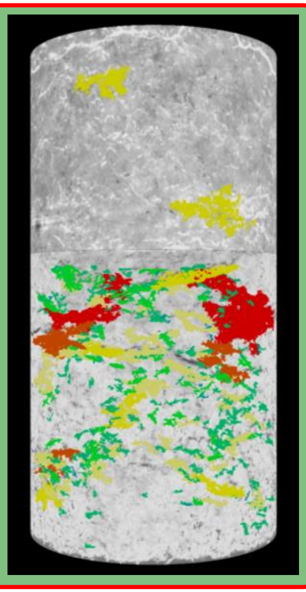

Voids (cracks) distribution in a rock salt sample from X-ray tomography

EVOLUTION OF APPARENT GAS PERMEABILITY WITH STRESS INCREASE

Under deviatoric loading

- At low confining pressure (1 MPa): small increase in gas permeability from the dilatancy threshold due to **microcracking damage**
- At high confining pressure (5 MPa): no increase in permeability because the material becomes **fully plastic** which practically eliminates microcracking and thus dilatancy

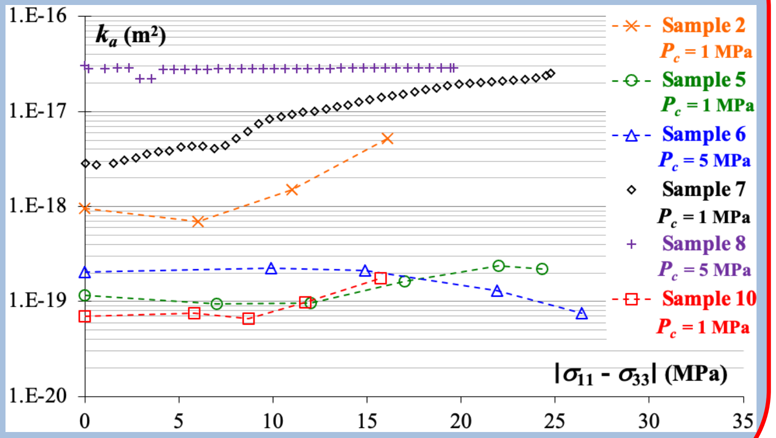

Evolution of apparent permeability k_a as a function of deviatoric stress

Under hydrostatic loading

- Gas permeability decreases because of the **closure of voids** (cracks and pores)
- Decrease is irreversible if time of run is high enough
- Due to the **self-healing process** (irreversible closure of cracks)

→ **Restoration of the permeability** of undisturbed natural rock salt

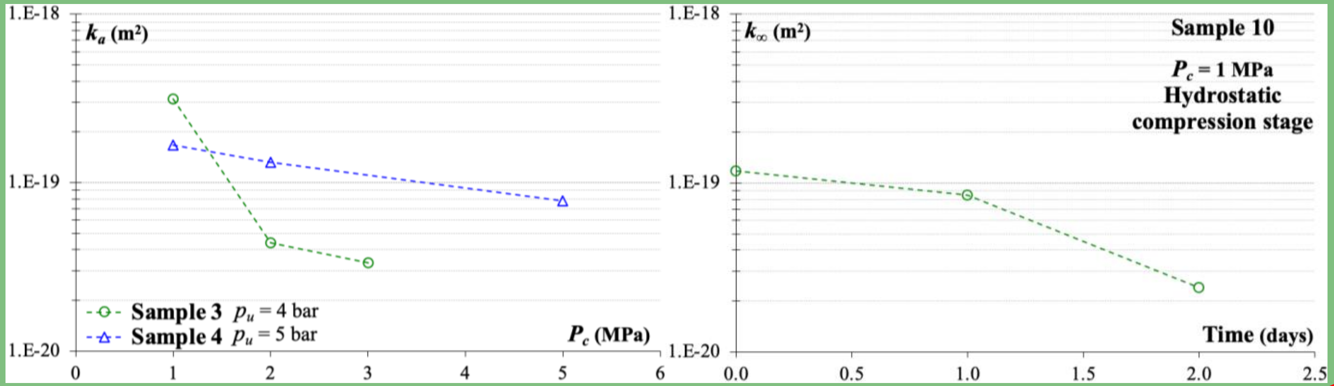

Evolution of apparent permeability k_a as a function of confining pressure *Pc* and time

IMPACT OF MECHANICAL AND THERMAL FATIGUE ON ROCK SALT PERMEABILITY

Static (creep test) and dynamic (cyclic) mechanical fatigue

- Volumetric dilatancy (microcracking damage) develops and increases slightly the permeability during dynamic fatigue
- Self-recovery reduces damage and decreases slightly the permeability during static fatigue (creep)

→ Different mechanisms involved in rock salt deformation during dynamic and static fatigue act in a competitive way to **annihilate any significant permeability evolution**

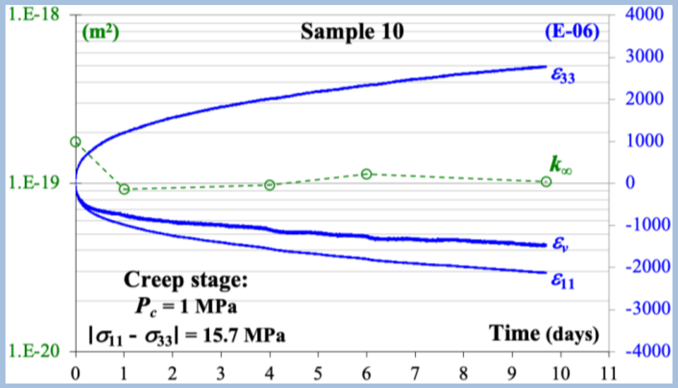

Evolution of permeability k and deformations as a function of time during a creep test

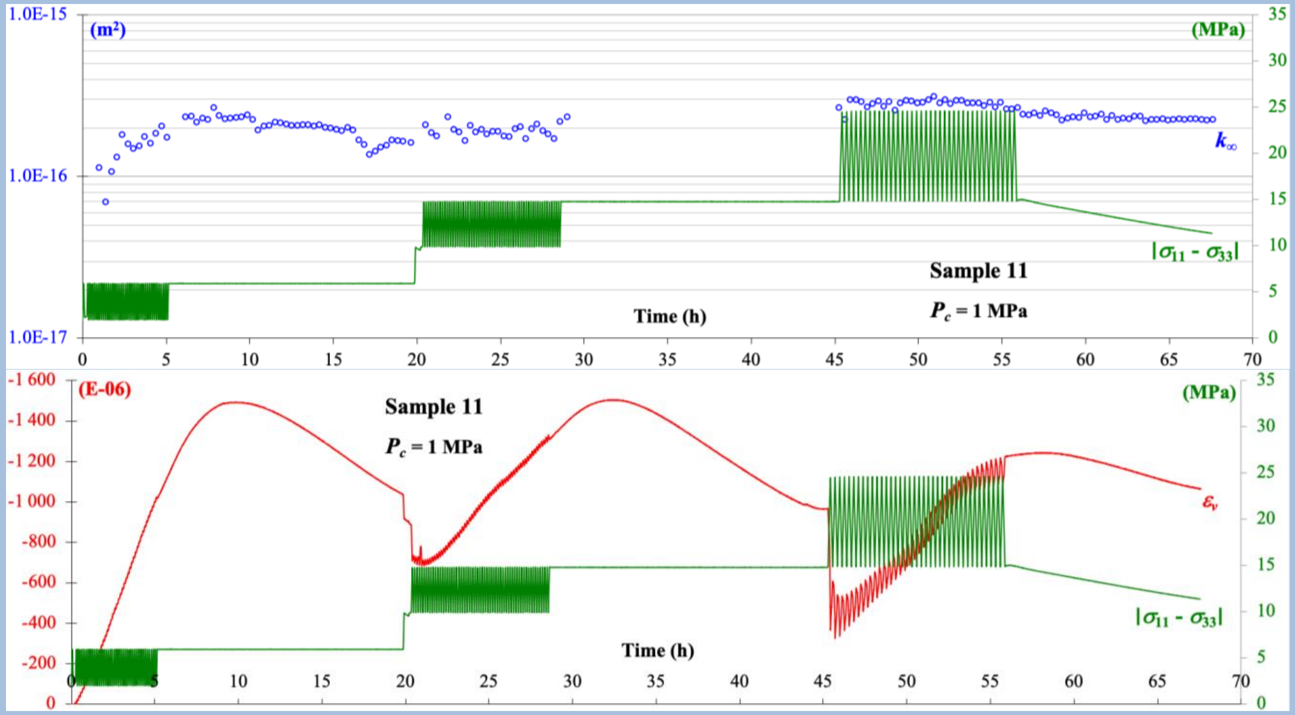

Evolution of permeability k and volumetric deformation ε_v as a function of time during the cyclic triaxial compression test

Cyclic thermal fatigue

- Small permeability increase due to the **microcracking damage** that develops at the **microscopic scale**
- Due to the **anisotropy of the thermal deformation** of rock forming minerals and to the **polycrystalline nature** of rock salt

→ Deformation heterogeneities and then differential thermal stresses and **microcracking damage**

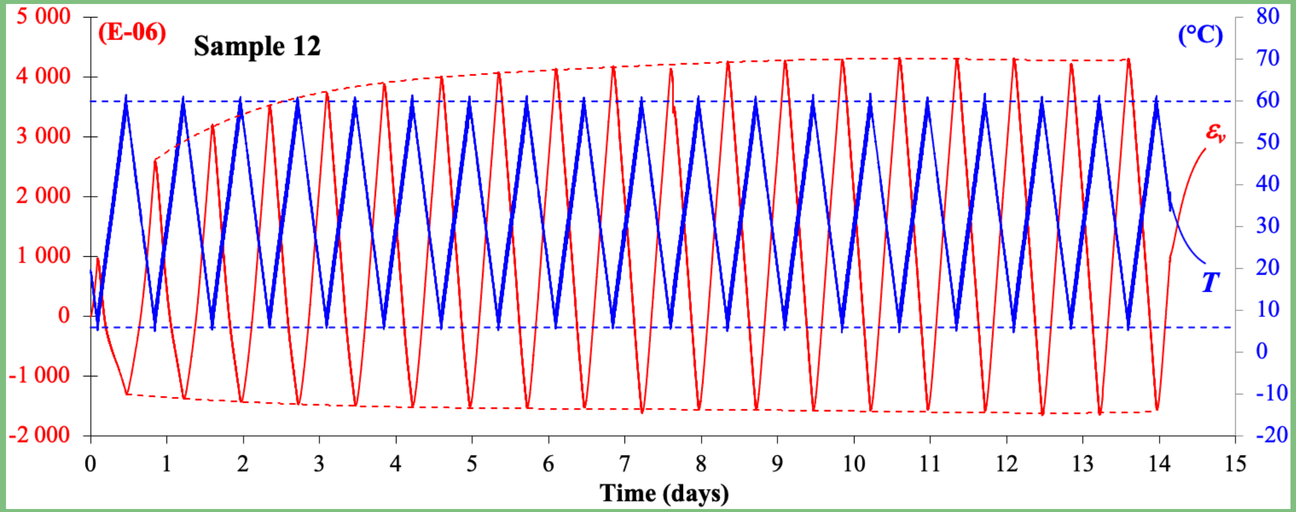

Evolution of volumetric deformation ε_v as a function of time during the thermal cyclic fatigue test

Evolution of apparent permeability k_a as a function of mean gas pressure, before and after the thermal cyclic fatigue test

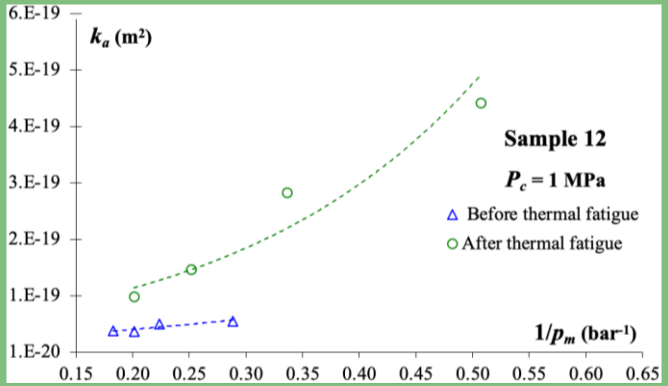

Intrinsic permeability

Before test: 2.7×10^{-20} m^2

After test: 4.9×10^{-20} m^2

EXPERIMENTAL HIGHLIGHTS

- Permeability of the studied rock salt varies over more than 4 orders of magnitude
- Slippage (Klinkenberg) effect only observed for the less permeable and damaged samples
- Deviatoric loading under low confining pressure (1 MPa)
  → Small increase in gas permeability from the dilatancy threshold due to microcracking
- Deviatoric loading under high confining pressure (5 MPa)
  → No increase in permeability because the material becomes fully plastic (no more microcracking)
- Hydrostatic loading
  → Gas permeability decreases because of irreversible cracks closure due to self-healing process
- Permeability increases slightly during dynamic/cyclic mechanical and thermal fatigue tests (corresponding to high-frequency cycling in salt caverns) due to microcracking
- Permeability decreases during static fatigue (creep) thanks to the self-recovery process
- Results have to be confirmed on less initially damaged salt samples !!!

The different mechanisms (viscoplasticity with strain hardening, microcracking and cracks healing) involved in rock salt deformation act in a competitive way to annihilate any significant permeability evolution.
→ Strong confidence in the H_2 storage in salt caverns which remains by far the SAFEST SOLUTION

Numerical modeling of hydrogen storage in salt cavern

- From available experimental results on salt rock, propose/develop a **rheological model that reproduces the main features of short and long term behavior**
- **Validation based on experimental tests and application(s) to salt cavern**
- Analysis of the impact of the operational phase:
  - ✓ Mechanical behaviour of the salt cavern
  - ✓ H_2 leakage through the cavern wall (extent of the dissolved H_2 plume)

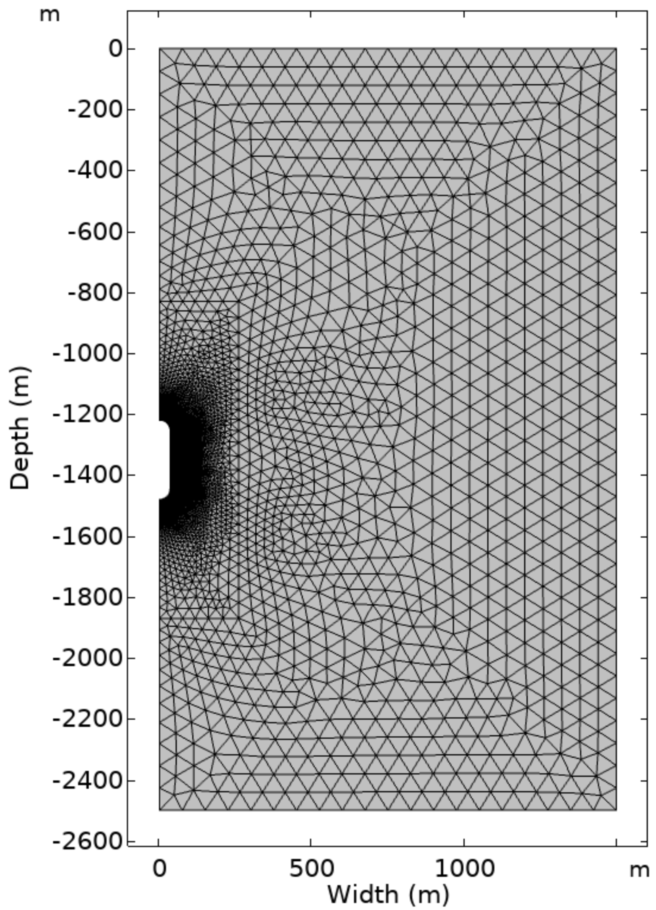

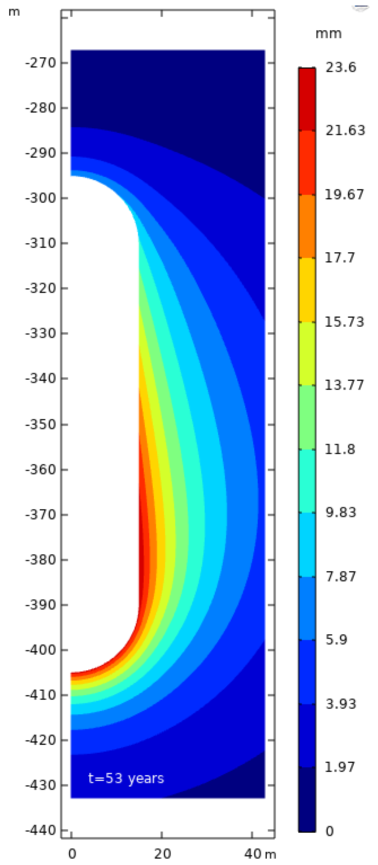

- **HydroMechanical model**: viscoplastic and damage model

Coarita-Tintaya E.D., Golfier F., Grgic D., Souley M. and Cheng L. *2023, Hydromechanical modelling of salt caverns subjected to cyclic hydrogen injection and withdrawal, Computers and Geotechnics, 162: 105690, [10.1016/j.compgeo.2023.105690]*

- **ThermoHydroMechanical model**: Previous model + fatigue + healing + thermal coupling

Elastoplastic and damage model

Elastic tensor

(compressive stresses are negative and $\sigma_1 \leq \sigma_2 \leq \sigma_3$)

$$C_{ijkl} = (1 - d)C^0_{ijkl}$$

$$d = d_i + d_f + d_t - h \qquad ; \qquad d \in [0; 1]$$

d_i: instantaneous damage
d_f: fatigue damage
d_t: tertiary damage
h: healing

d: total damage

Mohr-Coulomb yield surface

$$f_p = q + p\, M_p - N_p$$

$$M_p = \eta_p(\gamma^p) \frac{\sin\phi}{\left(\frac{\cos\theta}{\sqrt{3}} - \frac{1}{3}\sin\theta\, \sin\phi\right)} \quad ; \quad N_p = \eta_p(\gamma^p) \frac{(1 - d_i - d_f + h)\, c\, \cos\phi}{\left(\frac{\cos\theta}{\sqrt{3}} - \frac{1}{3}\sin\theta\, \sin\phi\right)}$$

Hardening rule

$$\eta_p(\gamma^p) = 1 - (1 - \eta_p^0)\exp\{-\alpha_p^0\, \gamma^p\}$$

Elastoplastic and damage model

Plastic potential

(Chiarelli *et al* 2003, Souley *et al.* 2017)

$$g = q + \beta(\gamma^p)\, p$$

$$\beta(\gamma^p) = \begin{cases} \beta_m - (\beta_m - \beta_0)\exp\left(-b_\beta\, \gamma^p\right) & ; \quad \gamma^p < \gamma^p_{ult} \\ \beta_{ult}\, \exp\left(1 - \dfrac{\gamma^p}{\gamma^p_{ult}}\right) & ; \quad \gamma^p \geq \gamma^p_{ult} \end{cases}$$

$$\beta_m = \begin{cases} \beta^0_m \exp\left(a_p\, \sigma_1\right) & ; \quad \sigma_1 < 0 \\ \beta^0_m & ; \quad \sigma_1 \geq 0 \end{cases}$$

$\beta(\gamma^p)$: dilatancy coefficient

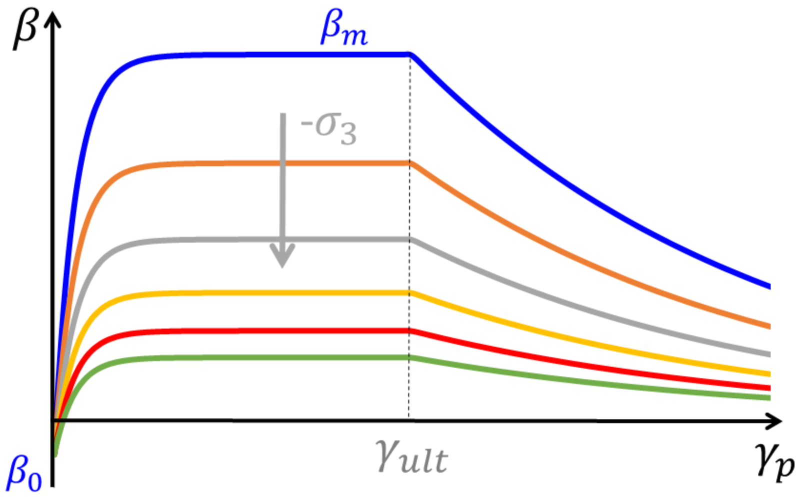

β_0 ($\beta_0 < 0$) is the initial volumetric contraction, β_m ($\beta_m > 0$) is the volumetric dilatancy at large deformation

We have volumetric contraction when $\beta < 0$, whereas the plastic strains evolve towards volumetric dilatancy if $\beta > 0$.

Elastoplastic and damage model

Instantaneous damage (d_i) (Mazars 1984)

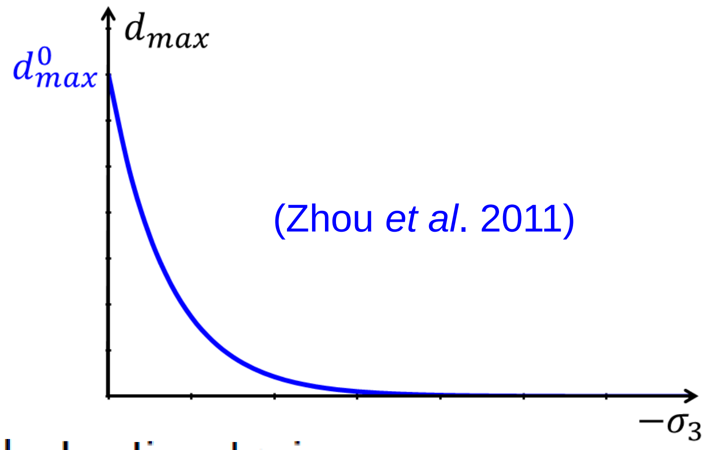

$$f_d = d_i^{max}\{1 - \exp[-b_d(Y_d - Y_0)]\} - d_i \leq 0 \quad ; \quad d_i \in [0; d_i^{max}]$$

$$d_i^{max} = \begin{cases} d_{i0}^{max} \exp(a_d \sigma_1) & ; \quad \sigma_1 < 0 \\ d_{i0}^{max} & ; \quad \sigma_1 \geq 0 \end{cases}$$

$Y_d = \sqrt{\langle \varepsilon \rangle : \langle \varepsilon \rangle}$; ε is the principal strain value of the elastic and plastic strains

a_d: parameter describing the effect of confining stress

Fatigue damage (d_f) (Zhang et al. 2023)

$$\dot{d}_f = \frac{b_f}{T_f}(d_f^{max} - d_f) \quad ; \quad d_f \in [0; d_f^{max}]$$

$$d_f^{max} = d_{f0}^{max}\,\eta_p \left(1 + b_{f2}\frac{\langle Y_d - Y_d^c \rangle}{Y_d^c}\right)$$

Assumption: The value of instantaneous damage is constant during the fatigue test

Elastoplastic and damage model

Creep strain rate

Transient creep (Kelvin-Voigt model)

Steady-state creep (Norton law)

$$\dot{\varepsilon}_{ij}^{c} = \left[\boxed{\frac{1}{\bar{\eta}_k^*}\left(q^* - \bar{G}_k^* \, \varepsilon_{tr}\right)} + \boxed{A_N \exp\left(-\frac{B_N}{T}\right)\left(\frac{q^*}{\sigma_{ref}}\right)^{n_N}} \right] \frac{3}{2}\frac{s_{ij}}{q}$$

$$\bar{G}_k^* = G_k \exp\left(k_1 \, q^*\right) \; ; \; \bar{\eta}_k^* = \eta_k \exp\left(k_2 \, q^*\right)$$

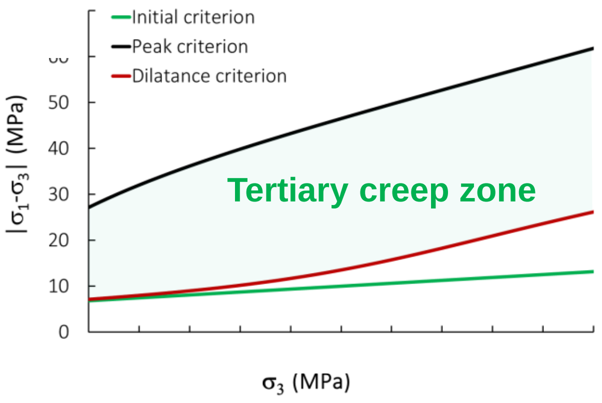

Tertiary damage (d_t)

(Hou *et al.* 2003)

$$\dot{d}_t = A_T \frac{A_T}{(1-d)^{n_T}} \left\langle \frac{f_{ds}}{\sigma_{ref}} \right\rangle^{n_T}$$

$$q^* = \frac{q}{1-d}$$

q^*: Mises stress undamaged

q : Mises stress damaged

➔Damage is activated and increases if the damage limit (dilatance criterion) is exceeded

Healing (h)

$$\dot{h} = \frac{d}{h_1} \left\langle \frac{-f_{ds}}{\sigma_{ref}} \right\rangle$$

Assumption: The healing boundary and the damage threshold are identical

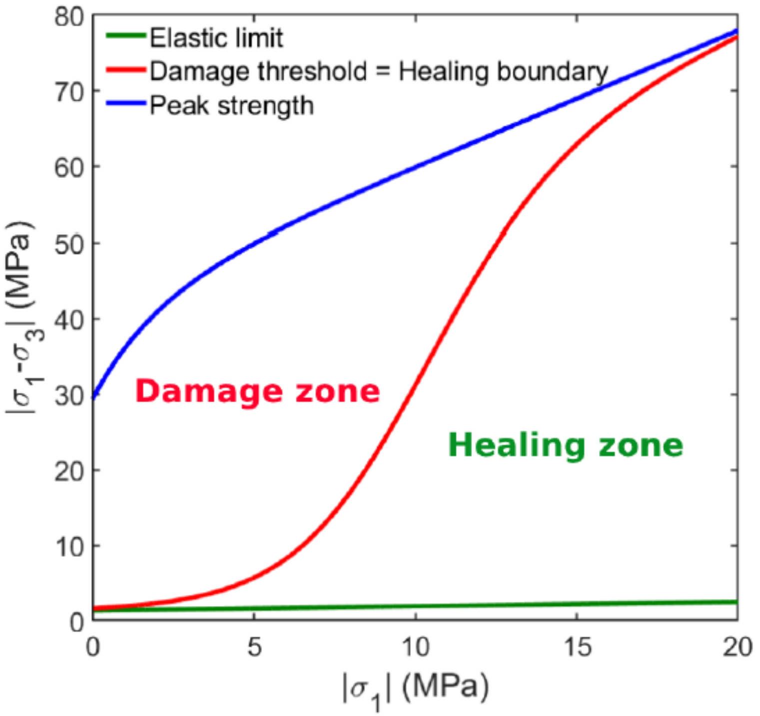

Mathematical formulation

Thermo-hydro-mechanical coupling

$$\nabla.[C:\varepsilon^e - b(p - p_{ref})I - \alpha C:(T - T_{ref})I] + \rho_m \vec{g} = 0$$

$$\rho_f b \frac{\partial \varepsilon_v}{\partial t} + \frac{\rho_f}{M}\frac{\partial p}{\partial t} + \nabla.(\rho_f \vec{q}) - 3\rho_f \alpha_m \frac{\partial T}{\partial t} = 0$$

$$\rho C_p \frac{\partial T}{\partial t} + \cancel{\rho_f C_{p,f} \vec{q}.\nabla T} - \nabla.(\lambda \nabla T) = 0$$

Where:

$$n\frac{\partial(c_{H_2})}{\partial t} + \nabla.(q_i\, c_{H_2}) = \nabla.(n\, \boldsymbol{D}^*.\nabla c_{H_2})$$

$$C = (1-d)C^0$$

$$\rho_m = (1-n)\rho_s + n\rho_f$$

$$\vec{q} = -\frac{k}{\mu_f(T)}(\nabla p + \rho_f \vec{g})$$

$$\frac{1}{M} = \frac{n}{K_f} + \frac{(1-b)(b-n)}{K_d}$$

$$\alpha_m = (b-n)\alpha + n\alpha_f(T)$$

$k = k_0 10^{A_k d}$ (Gawin *et al*. 2002)

- Fully water-saturated material
- Two-phase flow not considered
- Dissolved H_2 transport by advection and diffusion
- The value of the Biot coefficient is 0.3 if material is damaged

Storage in salt cavern : case study

boundary and initial conditions

			Cavern A	Cavern B
Model geometry	Depth	m	-350	-1350
	Volume	m^3	70 686	910 800
H_2 Conditions	Pmax - H2	MPa	5	20
	Pmin - H2	MPa	2	6

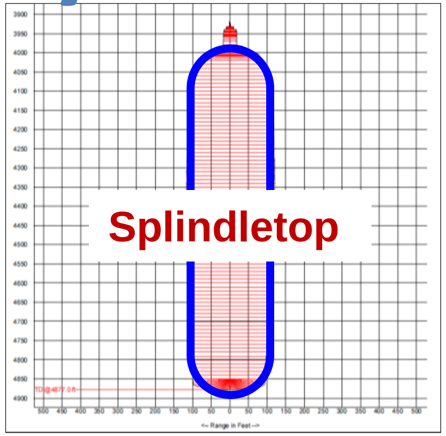

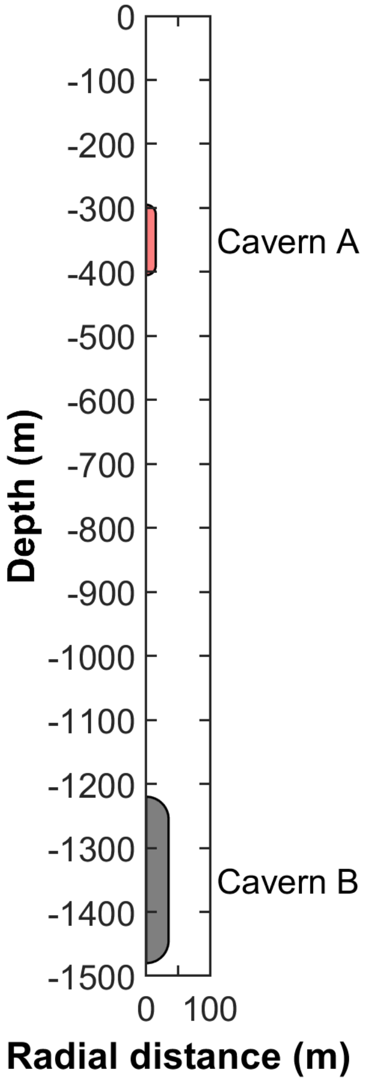

Cycling scenarios:

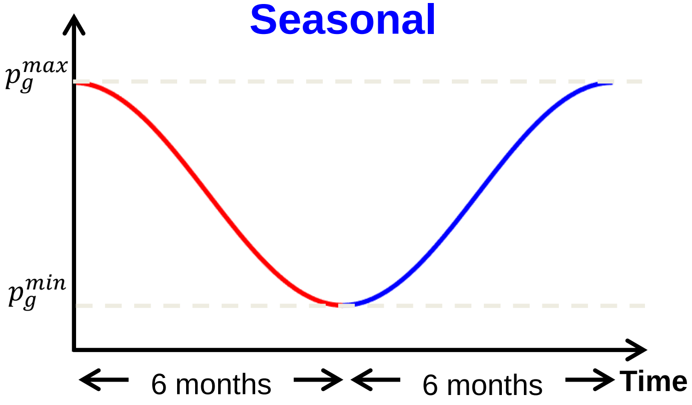

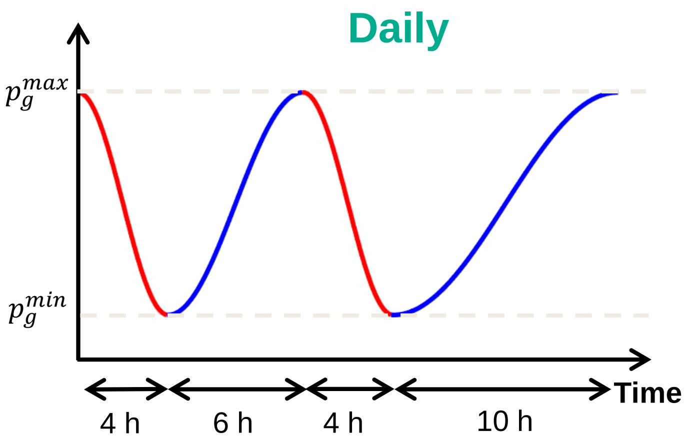

➔ For 50 years

➔ For 100 days

Analysis cases

- **Elastic (➔ To verify the HM model: realised)**
- **Cavern A (seasonal & daily)**
- **Cavern B (seasonal & daily)**

Storage in salt cavern : case study

Cavern geometry, boundary and initial conditions and properties

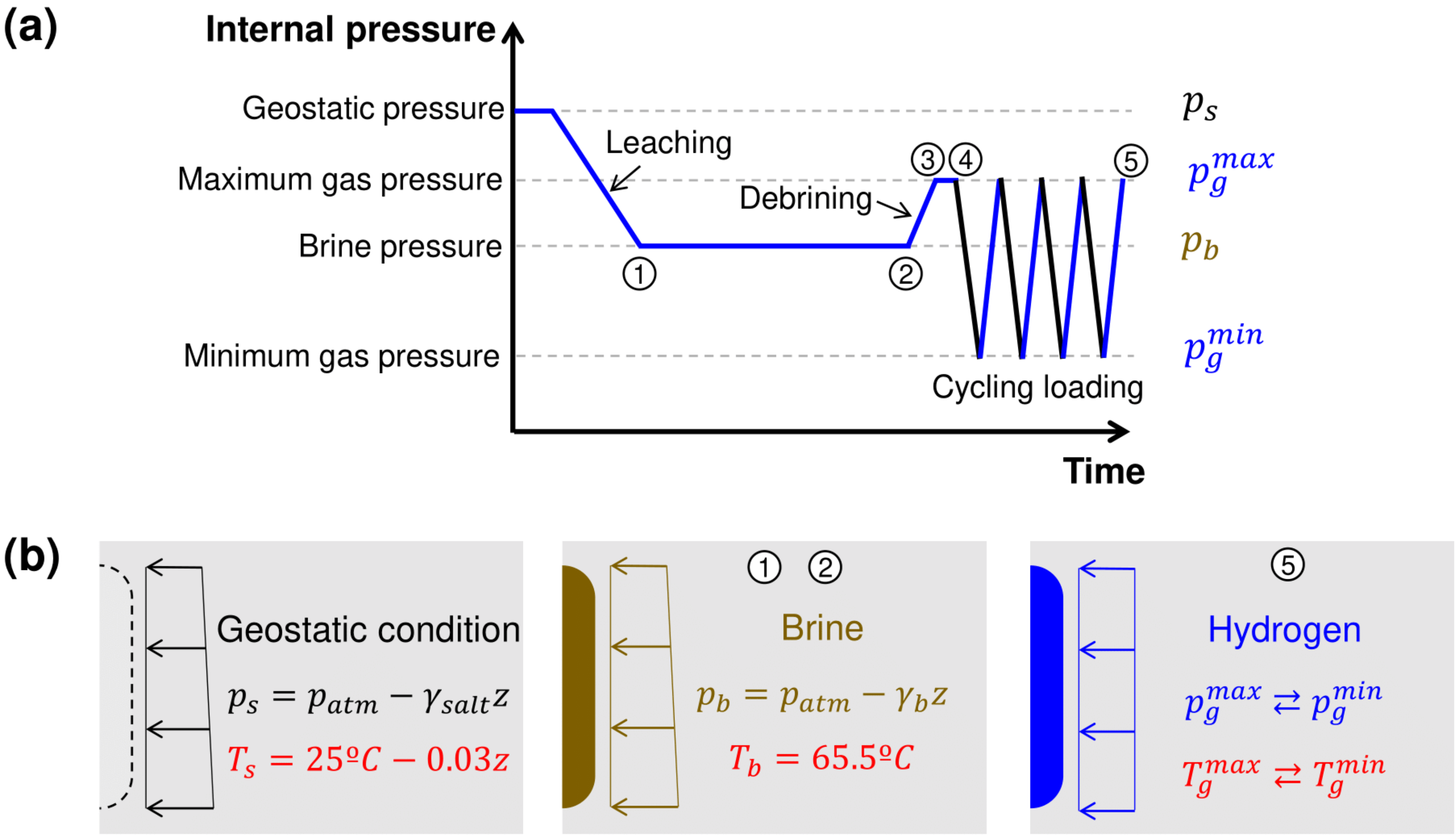

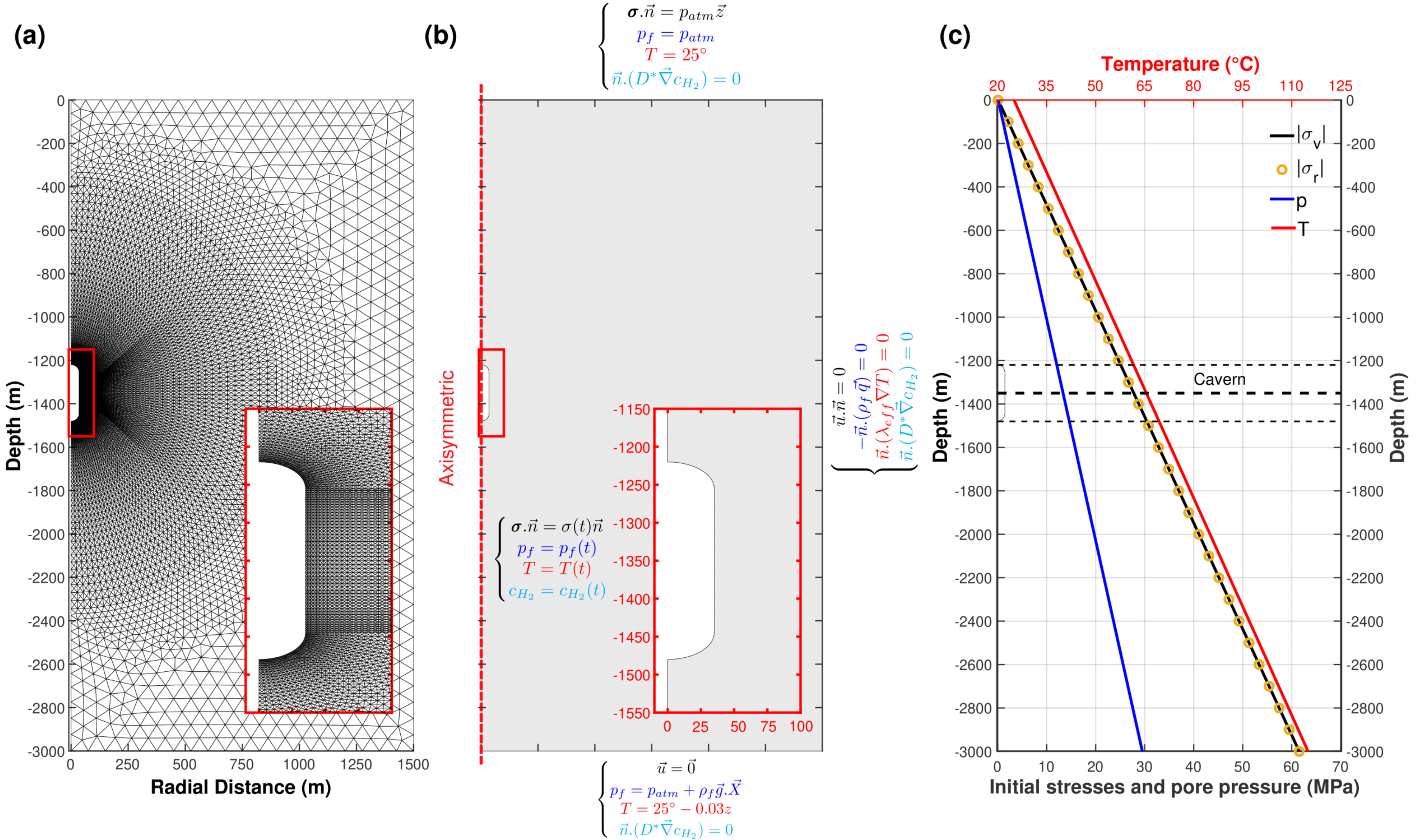

(a)
(b)
(c)
Depth (m)
Radial Distance (m)
Axisymmetric
$\boldsymbol{\sigma}.\vec{n} = p_{atm}\vec{z}$
$p_f = p_{atm}$
$T = 25°$
$\vec{n}.(D^*\vec{\nabla}c_{H_2}) = 0$
$\boldsymbol{\sigma}.\vec{n} = \sigma(t)\vec{n}$
$p_f = p_f(t)$
$T = T(t)$
$c_{H_2} = c_{H_2}(t)$
$\vec{u}.\vec{n} = 0$
$-\vec{n}.(\rho_f\vec{q}) = 0$
$\vec{n}.(\lambda_{eff}\vec{\nabla}T) = 0$
$\vec{n}.(D^*\vec{\nabla}c_{H_2}) = 0$
$\vec{u} = \vec{0}$
$p_f = p_{atm} + \rho_f\vec{g}.\vec{X}$
$T = 25° - 0.03z$
$\vec{n}.(D^*\vec{\nabla}c_{H_2}) = 0$
Temperature (°C)
Cavern
$|\sigma_v|$
$|\sigma_r|$
p
T
Initial stresses and pore pressure (MPa)

Storage in salt cavern : case study

Cavern geometry, boundary and initial conditions and properties

Short-term numerical values

Parameter	Value	Unit	Parameter	Value	Unit	Parameter	Value	Unit	Parameter	Value	Unit
E	35.0	GPa	α_p^0	70		a_p	0.5	1/MPa	d_{f0}^{max}	0.031	
ν	0.3		β_0	-0.02		b_d	70		b_f	0.036	s
c	12.5	MPa	β_m^0	1.5		d_{i0}^{max}	0.3		b_{f2}	1	
ϕ	28.3	°	b_β	80		a_d	0.5	1/MPa	Y_d^c	0.0278	
η_p^o	0.05		γ_{ult}^p	0.09		R_t	3	MPa	T_f	1	y

Long-term numerical values

Parameter	Value	Unit	Parameter	Value	Unit	Parameter	Value	Unit
G_k	12600	MPa	η_k	60000	MPa.d	n_T	3.5	
k_1	-0.18	1/MPa	k_2	-0.15	1/MPa	A_d	4.0E-10	1/d
l_1	0	1/K	A_N	0.005	1/d	β_{d0}	1	
G_{kE}	7560	MPa	B_N	4700	K	a_t	0.5	1/MPa
k_{1E}	-0.18	1/MPa	n_N	4		h_1	6000	d
l_{1E}	0	1/K	A_T	4.0E-8	1/d	β_h	1	

Storage in salt cavern : case study

Cavern geometry, boundary and initial conditions and properties

Hydraulic			Thermal			Transport		
Parameter	Value	Unit	Parameter	Value	Unit	Parameter	Value	Unit
k_0	1.0E-20	m^2/s	λ	6.8	W/(m.K)	D^*	6.0E-9	m^2/s
A_k	90		α	4.0E-5	1/K			
μ_f	0.001	Pa.s	C_p	850	J/(kg.K)			
n	0.012		α_f	$f(T)$	1/K			
b	0.012							
K_f	2.2E+9	Pa						
ρ_f	1000	kg/m^3						

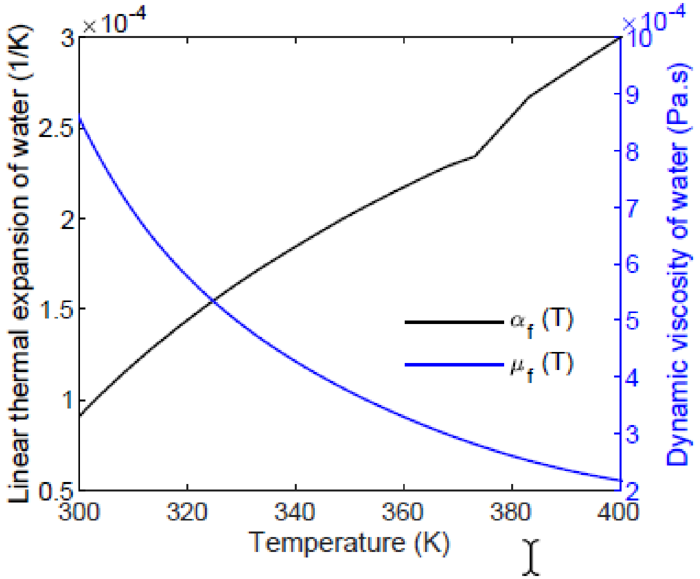

Hydro-mechanical results

Stress path at the bottom of the cavern (Deviatoric stress projected to the plane $\boldsymbol{\theta = \pi/6}$)

Seasonal

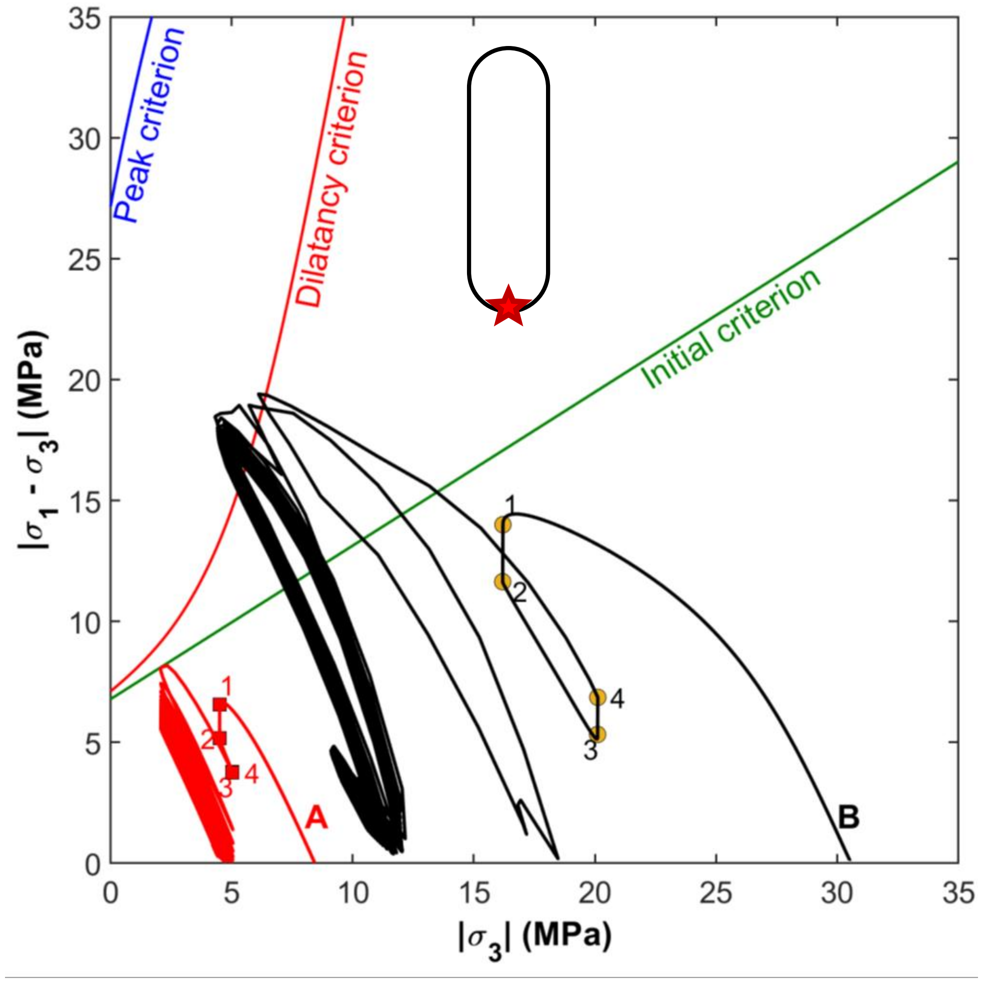

Daily

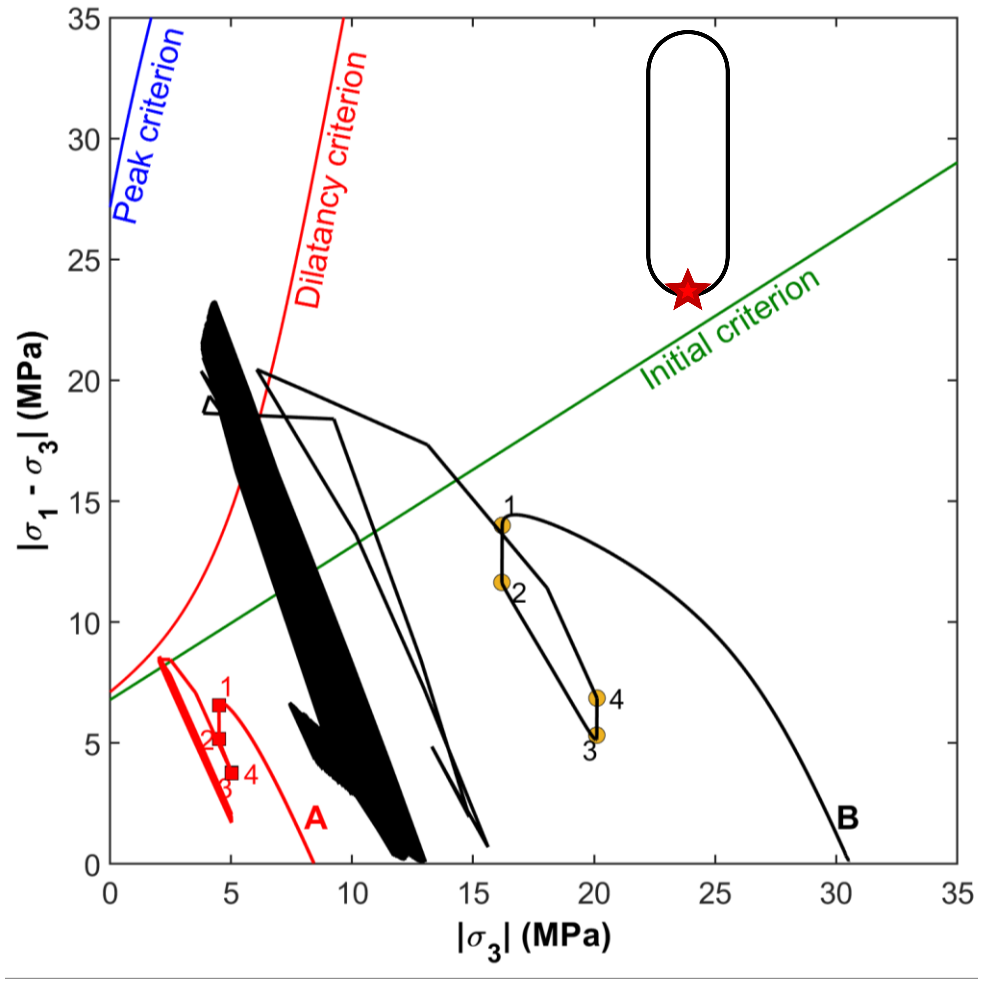

- Relaxation of deviatoric stresses over time
- **Seasonal and cavern A:** in the first extraction it exceeds the elastic limit. For the following cycles this limit is not exceeded due to creep. In **cavern B** the dilatancy criterion is reached

Hydro-mechanical results

Plastic and damage zone

Cavern A

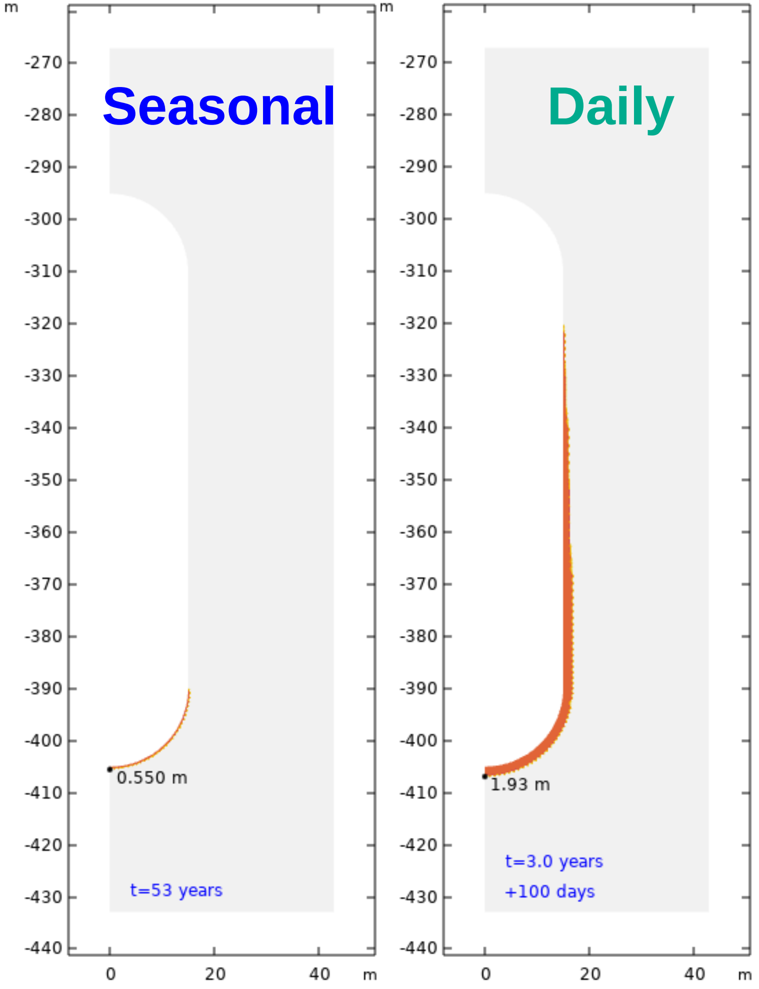

Cavern B

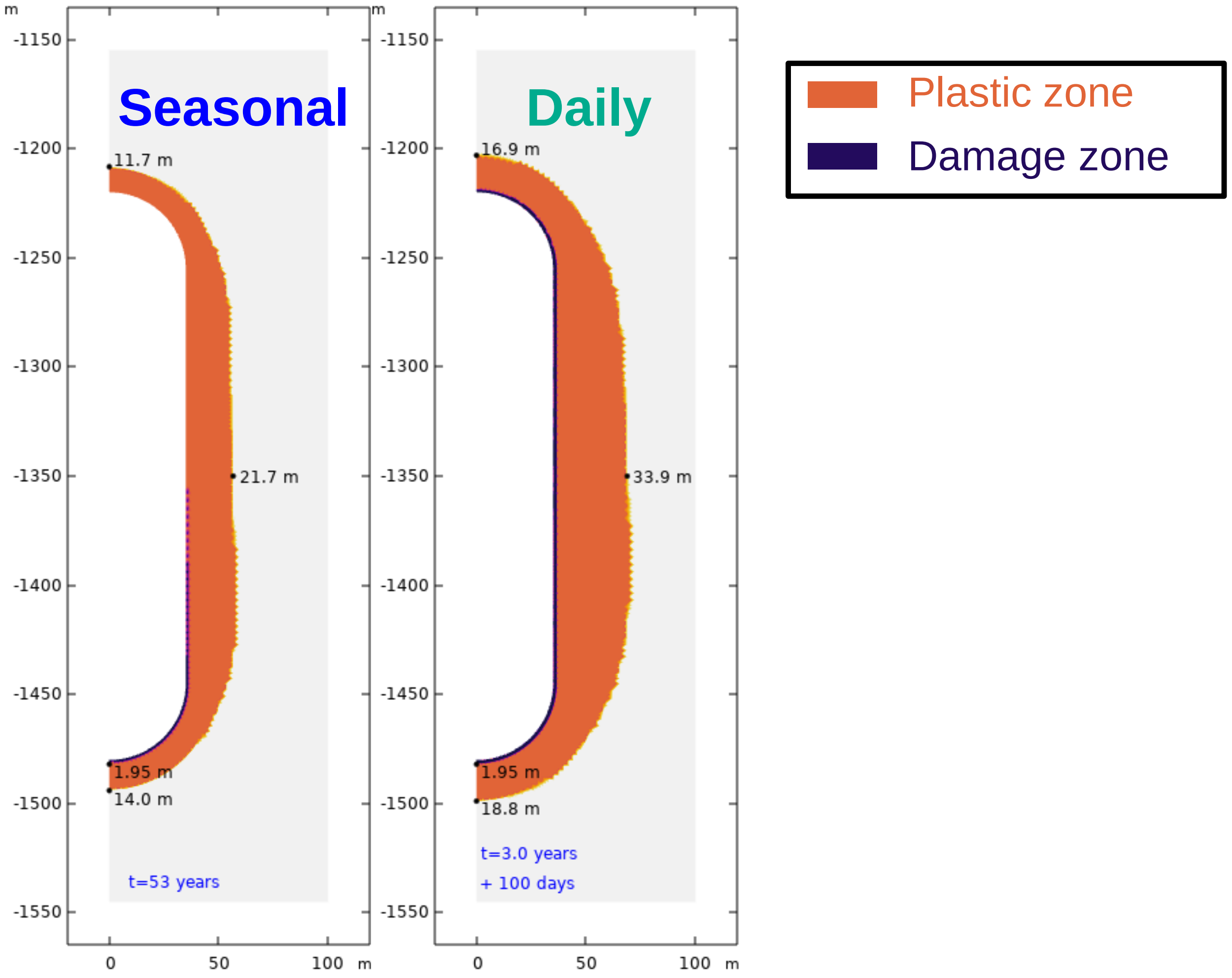

Around **cavern A** there is a small extension of the plastic zone, in the lower and lateral part of the cavern.

Around **cavern B**, the damage zone is initially located at the bottom. The plastic zone is all around the cavern and is more extensive for daily cycling

Hydro-mechanical results

Cavern wall displacements

Cavern A **Cavern B**

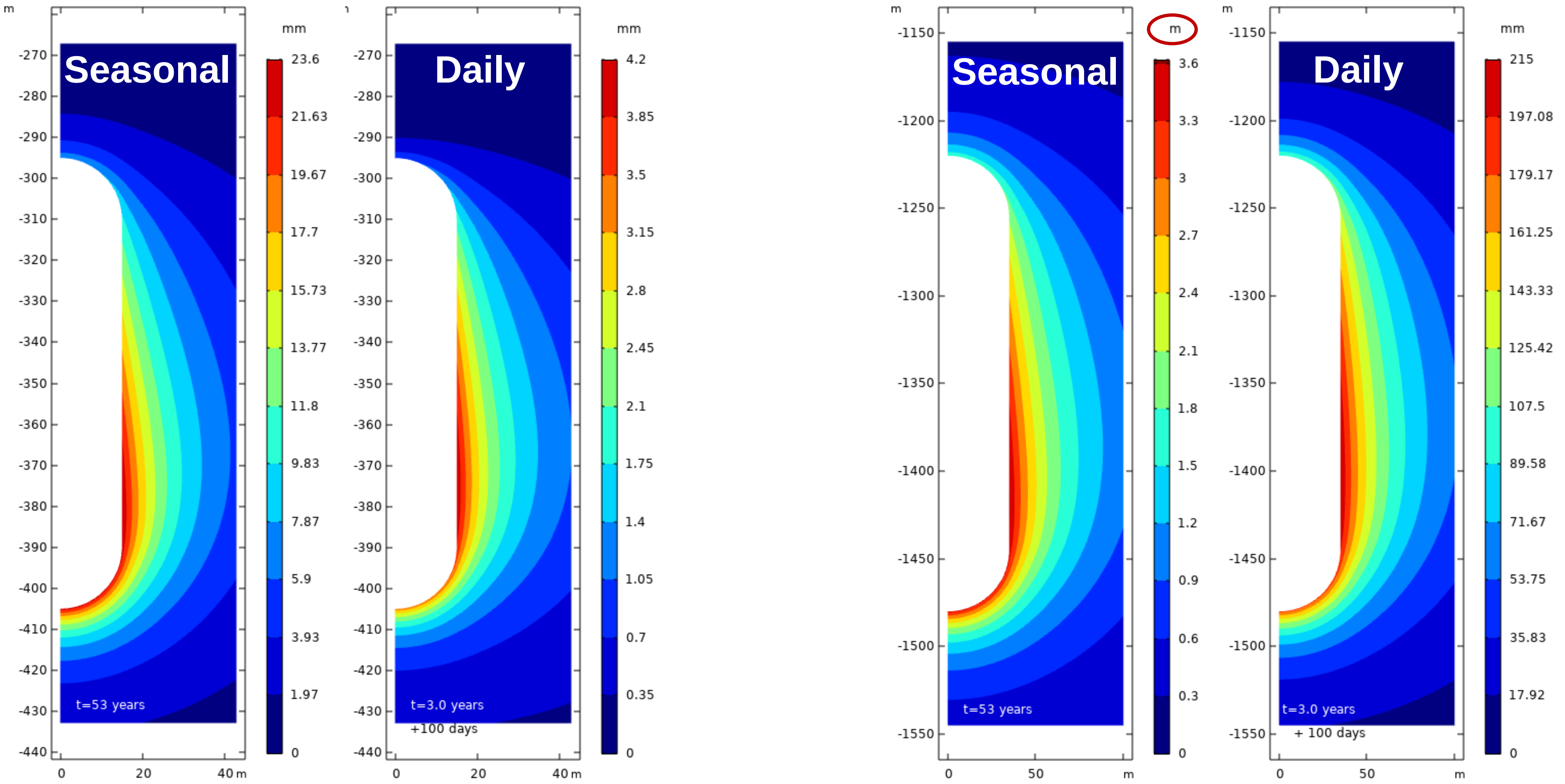

Around **cavern A**, the displacements are small and in the order of 26 mm

Around **cavern B**, the displacements are important for seasonal cyclage. Maximum displacement of 3.6 m on the lateral side

Hydro-mechanical results

Hydrogen leakage

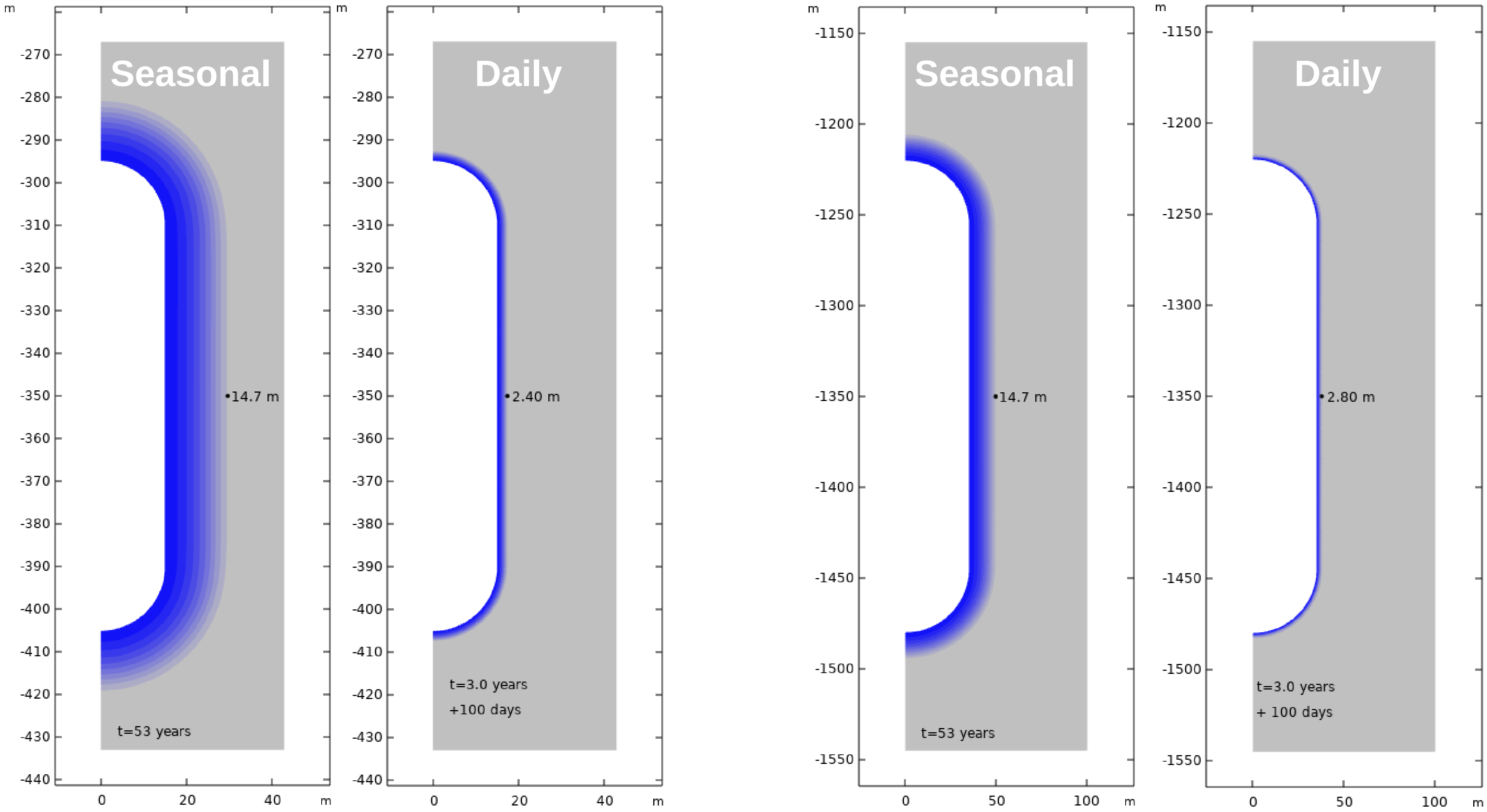

For both caverns, a similar hydrogen extension is estimated around the cavern. Almost 2.5 m for a daily cycling and almost 15 m for a seasonal cycling. **Gas transport mainly by diffusion**.

Thermo-hydro-mechanical results

Plastic and damage zones around cavern

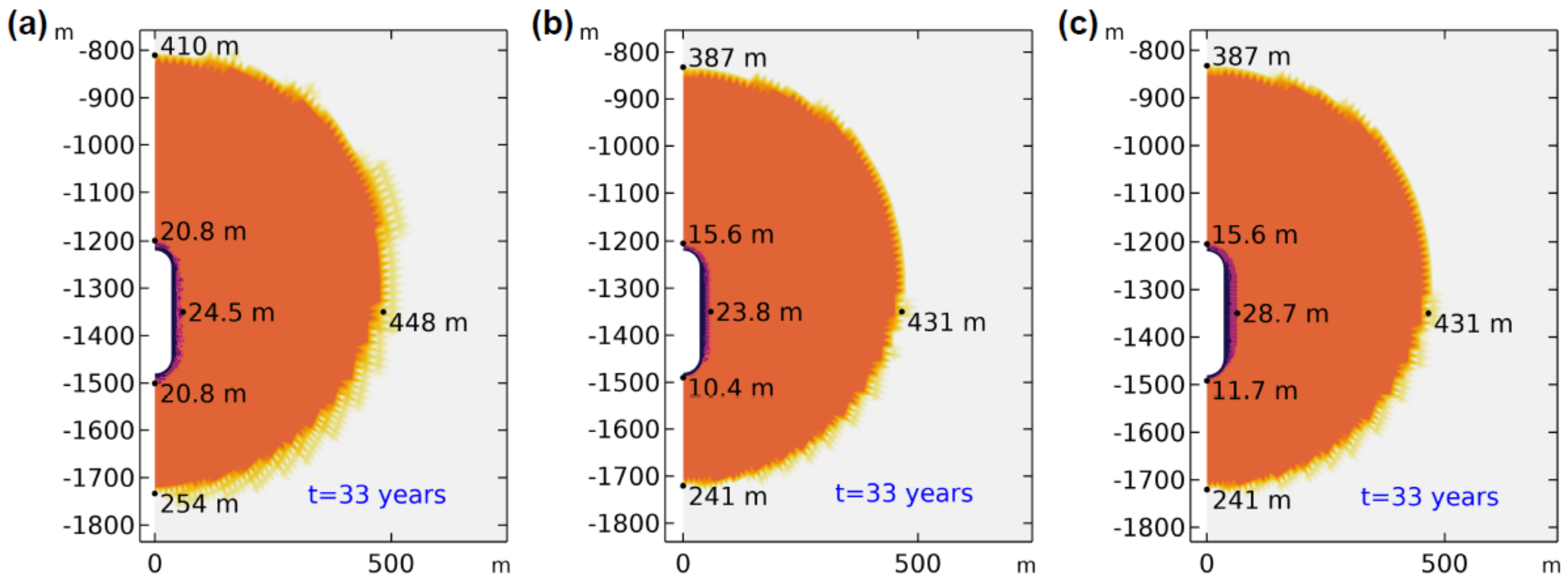

Zones at 33 years for (a) **Case 1**: HM (b) **Case 2**: THM (c) **Case 3**: THM (without healing)

- Before the operation phase, only plastic zones are calculated in the analysis cases
- At 3.5 years (first minimum gas pressure), the damage zone appears, and the plastic zone increases
- In the following years, damage zones increased slightly in extension, while the plastic zone increased more

Thermo-hydro-mechanical results

Net damage at the bottom of the cavern

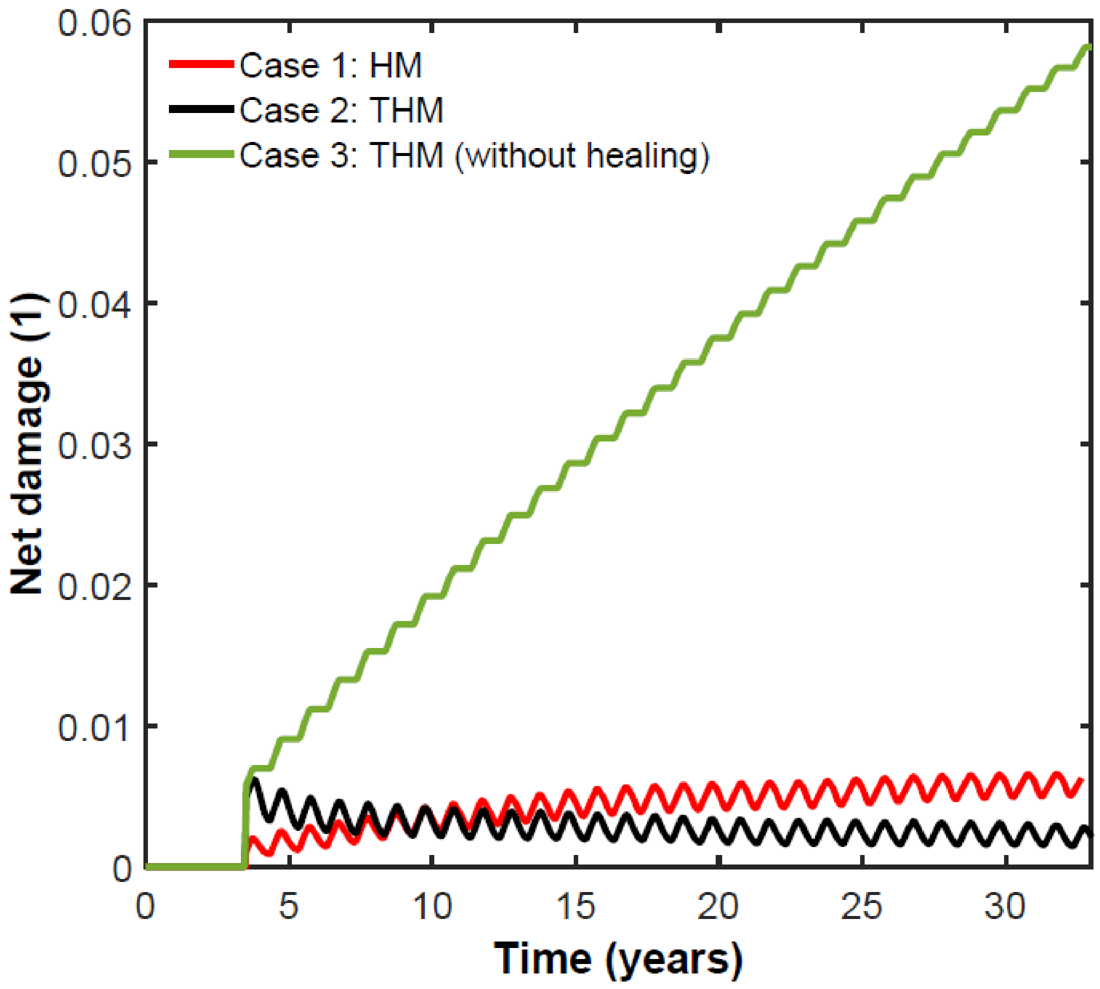

Note: Net damage is defined as $d = d_i + d_f + d_t - h$

Thermo-hydro-mechanical results

Cavern wall displacements

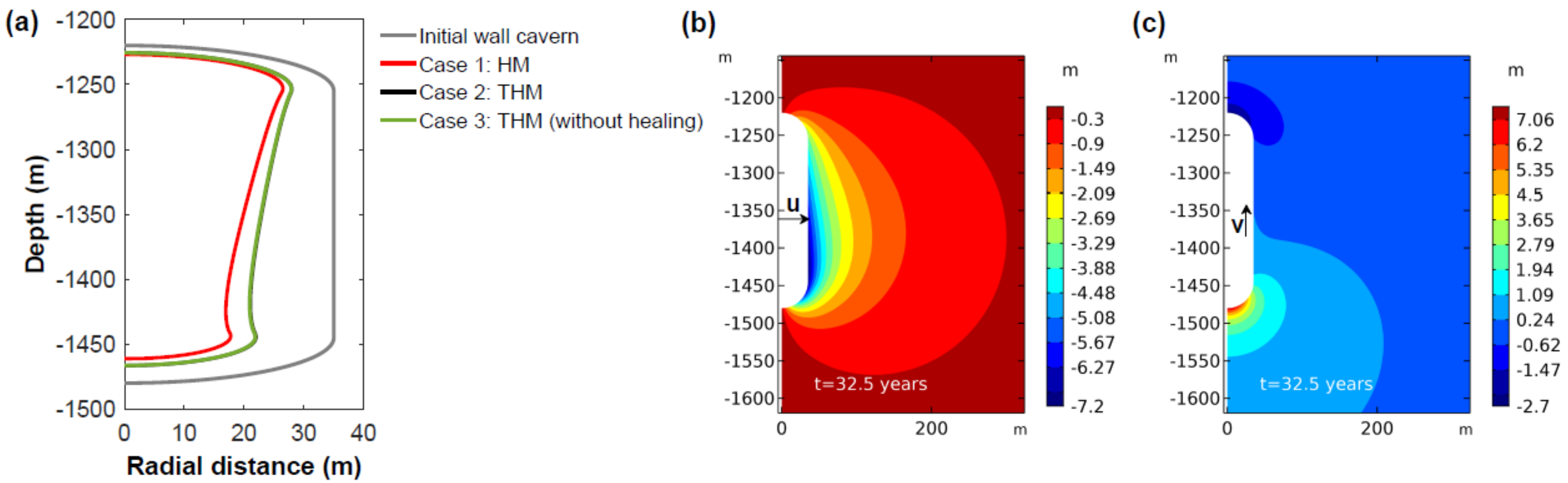

(a) Cavern wall displacements (scaled by a factor of 2.5), (b) horizontal and (c) vertical displacements for **Case 1**: HM

- Case 1 has more displacements than Cases 2 and 3 because it has a larger extent of the plastic zone around the cavern
- Cases 2 (THM) and 3 (THM without healing) exhibit similar displacements
- Important horizontal displacements are calculated on the bottom wall of the cavern, while significant vertical displacements are calculated on the floor of the cavern

Thermo-hydro-mechanical results

Pore pressure distribution

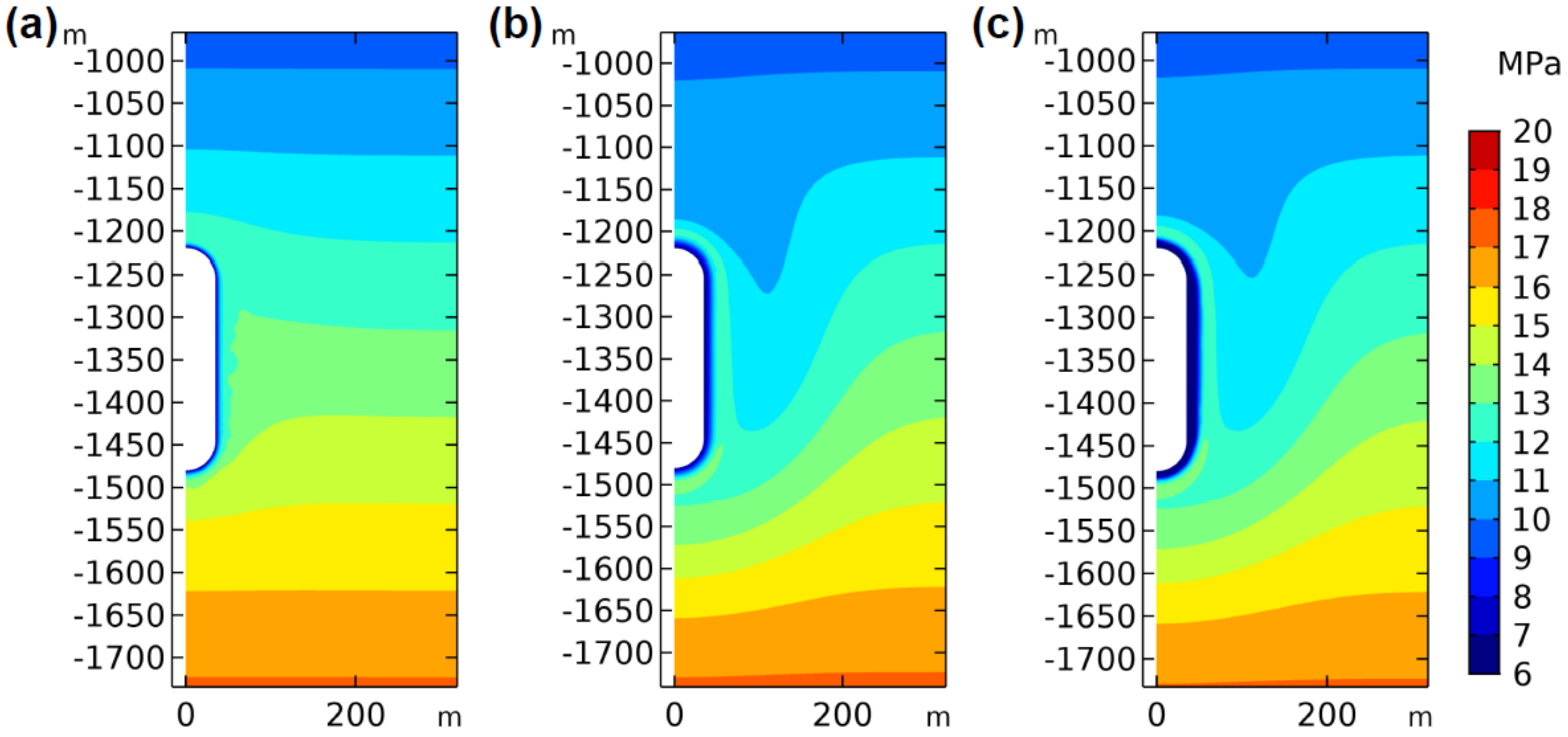

Pore pressure distribution around salt cavern at 32.5 years for:
(a) **Case 1**: HM (b) **Case 2**: THM (c) **Case 3**: THM (without healing)

- Pore pressure distributions for Cases 2 and 3 show more modification around the cavern compared to Case 1, due to the temperature effect.

Thermo-hydro-mechanical results

Hydrogen leakage

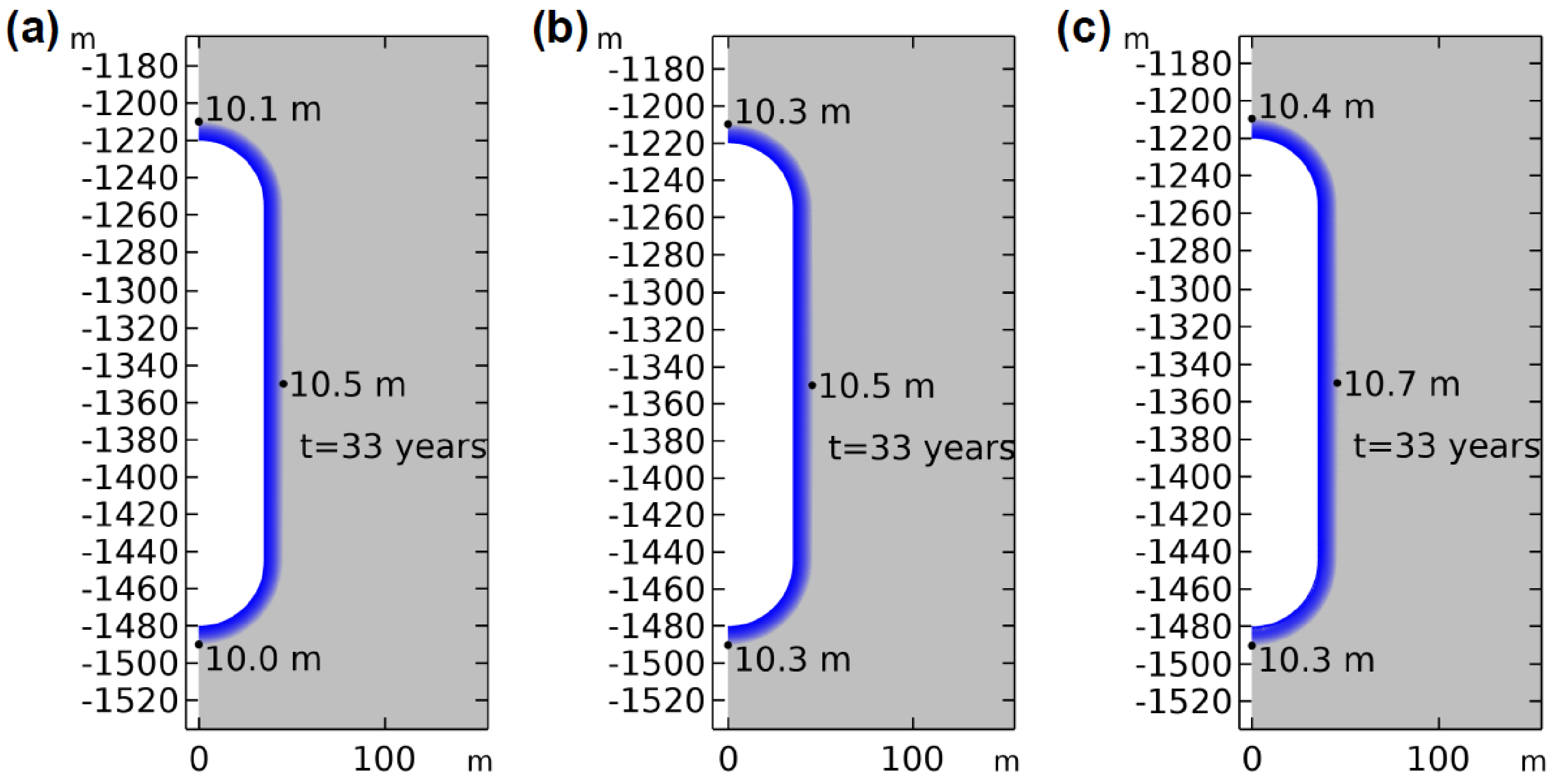

Hydrogen extension around salt cavern at 33 years for:
(a) **Case 1**: HM (b) **Case 2**: THM (c) **Case 3**: THM (without healing)

- Hydrogen extensions are similar for the three cases due to transport properties, modified only near the cavern wall

Conclusions

- **A THM model describing the main key features of the rock salt behavior has been developed**
  - ✓ **Short term model** takes into account elastoplastic and instantaneous damage behaviors
  - ✓ For the **long-term behavior**, the three creep phases generally observed on creep tests are considered
  - ✓ **Fatigue damage** and **healing** have been also implemented
  - ✓ **Thermal coupling** and **hydrogen transport** are considered

- **Numerical simulation results**
  - The **deep cavern** is more susceptible to mechanical stability problems.
  - The **daily scenario** is also **more detrimental** to the stability.
  - Even if damage occurs, the extent of damage zone is limited
  - the **amount of gas leakage is also limited** and both caverns lead to almost the same plume size because of diffusion which is preponderant.
  - Healing contributes to **annihilate any significant damage evolution**

Thank you for your attention !

Main assumptions of the model

- Rock salt is considered as an isotropic material
- Its elastic limit is very low -> The initial yield strength is assumed to be a fraction of the peak strength criterion
- It has a **hardening deformation mechanism** and shows a more **ductile response** than most other rocks
- **Ductile behaviour:** increasing confining stress
- Significant dilatancy at low confining stresses -> **To define the dilatancy criterion**
- we use the plastic potential: volumetric plastic strain (ε_v^p)
- if $\dot{\varepsilon}_v^p > 0$: we suppose that the material is in volumetric dilatancy

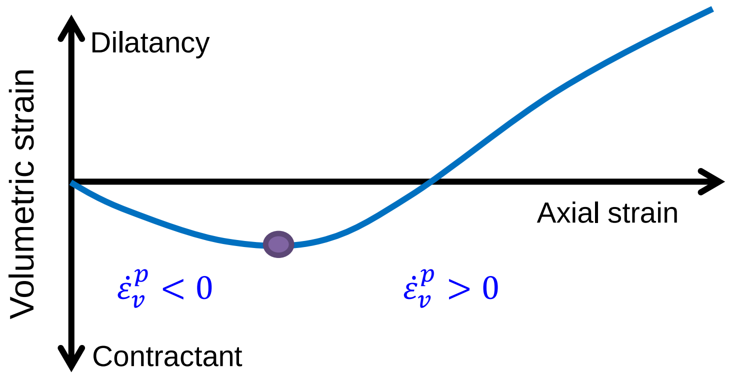

❖ **Damage initialisation:** volumetric dilatation, due to microcracking, lead to a significant increase in the permeability of rock salt

➔ Damage initiation is characterised macroscopically by dilatancy

➔ The maximum achievable damage is reduced with increasing confining stress, because there is no volumetric dilatancy ➔ ductile behaviour

➔ Based on continuum of damage mechanics - CDM, an **isotropic damage** variable is considered, in first approximation, which modifies the elasticity and strength parameters

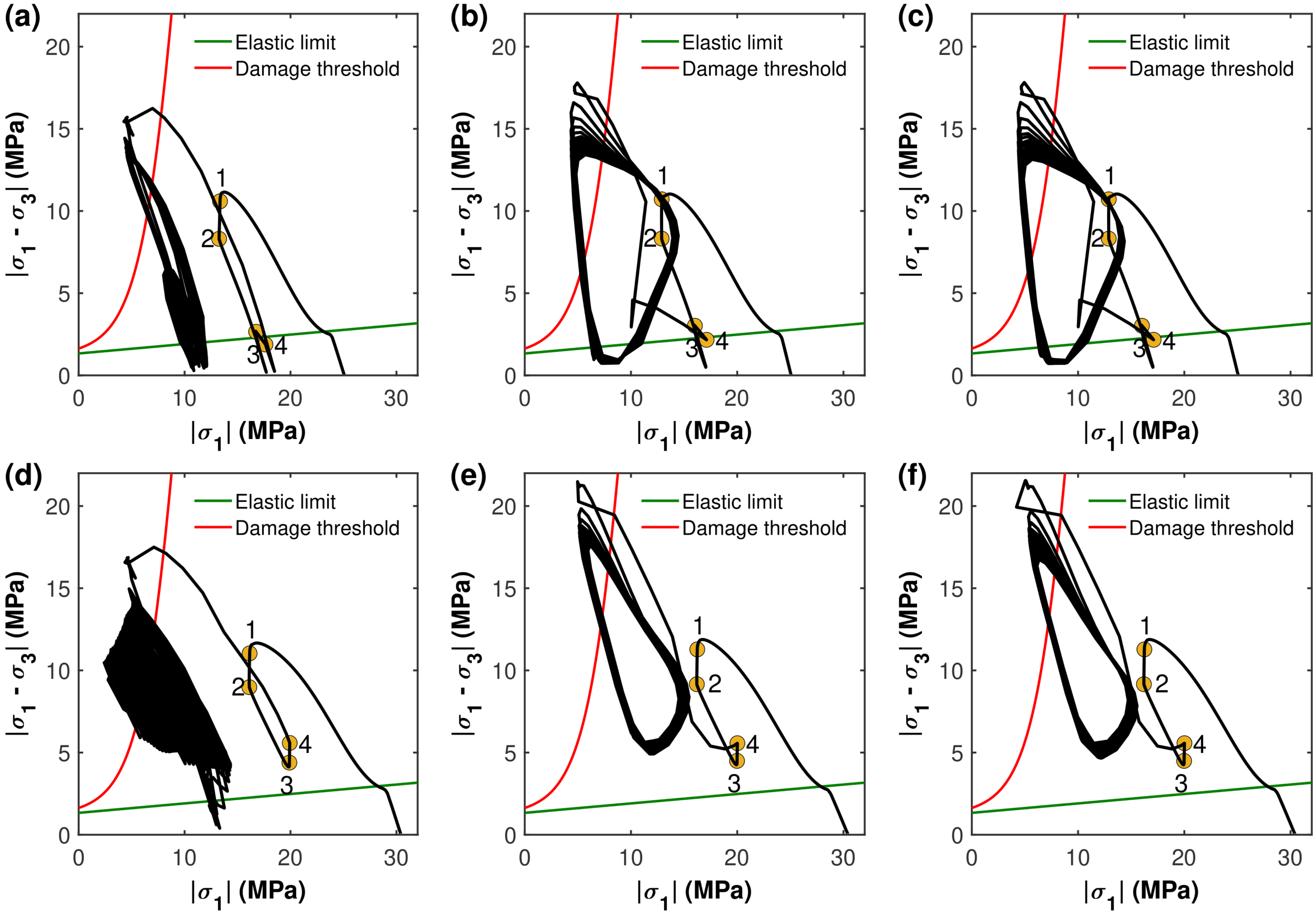

(a)
(b)
(c)
(d)
(e)
(f)
Elastic limit
Damage threshold
$|\sigma_1 - \sigma_3|$ (MPa)
$|\sigma_1|$ (MPa)
1
2
3
4

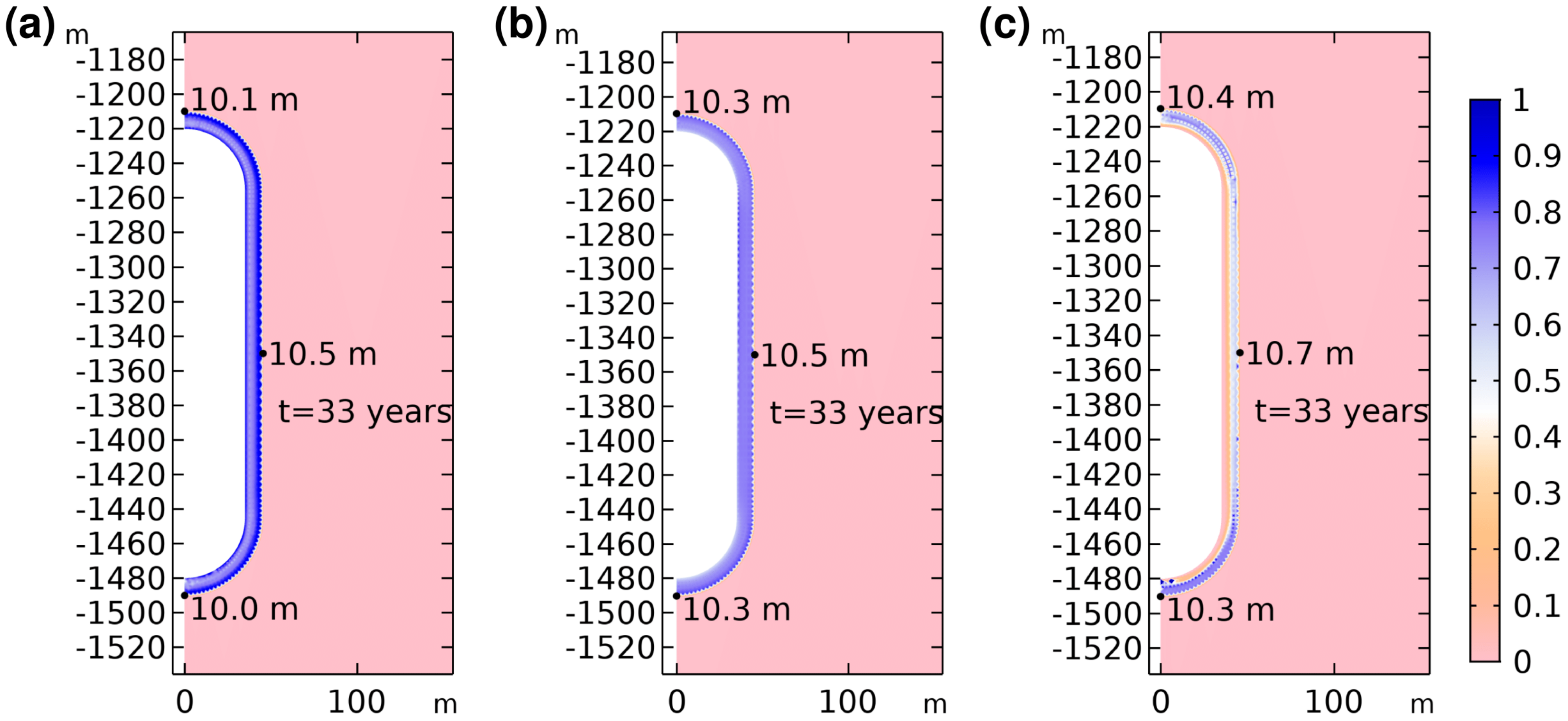
(a)
(b)
(c)
10.1 m
10.5 m
10.0 m
10.3 m
10.5 m
10.3 m
10.4 m
10.7 m
10.3 m
t=33 years
m
-1180
-1520
0
100
1
0.5
0

Proposed elastoplastic damage model

Full model equations

(compressive stresses are negative and $\sigma_1 \leq \sigma_2 \leq \sigma_3$)

M-C yield surface:

$f(p, q, \theta)$

$$f_p = q + pM_p - N_p$$

$$M_p = \eta^p(\gamma_p)\frac{\sin\phi}{\left(\frac{\cos\theta}{\sqrt{3}} - \frac{1}{3}\sin\theta\sin\phi\right)} \quad ; \quad N_p = \eta^p(\gamma_p)\frac{(1-d)c_i\cos\phi}{\left(\frac{\cos\theta}{\sqrt{3}} - \frac{1}{3}\sin\theta\sin\phi\right)}$$

Hardening variable: $\eta^p(\gamma_p) = \left\{\eta_o^p + \{1-\eta_o^p\}\frac{\gamma_p}{\alpha^p + \gamma_p}\right\}$ (Chiarelli *et al.* 2003, Zhou *et al.* 2011)

Plastic potential: $g = q + \beta(\gamma_p)p$ (Chiarelli *et al* 2003, Souley *et al.* 2017)

$$\beta(\gamma_p) = \begin{cases} \beta_m - (\beta_m - \beta_0)\exp(-b_\beta\gamma_p) & ; \quad \gamma_p < \gamma_{ult} \\ \beta_{ult}\exp\left(1 - \frac{\gamma_p}{\gamma_{ult}}\right) & ; \quad \gamma_p \geq \gamma_{ult} \end{cases}$$

$$\beta_m = \beta_{m0}\exp(a_d\sigma_3)$$

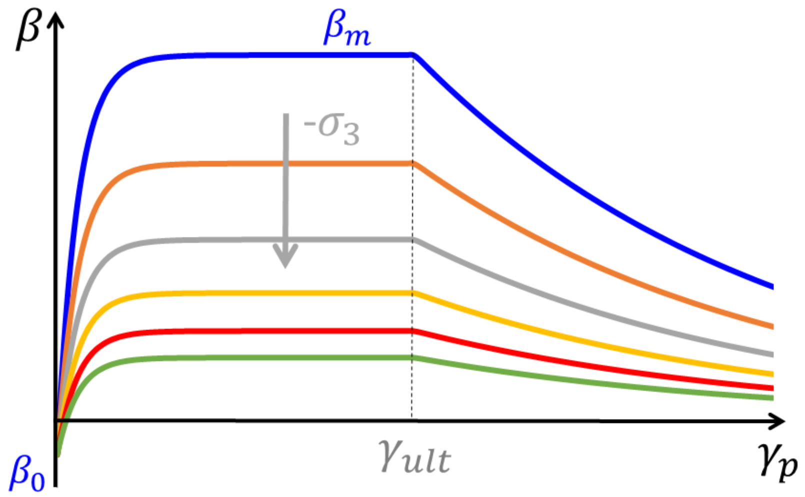

Rock salt behaviour in long-term

$$\dot{\varepsilon}_{ij}^{c} = \left(\frac{1}{\bar{\eta}_k^*} \left(q^* - \bar{G}_k^* \varepsilon_{tr} \right) + A_N \left(\frac{q^*}{\sigma_{ref}} \right)^{n_N} \right) \frac{3}{2} \frac{s_{ij}}{q^*}$$

$$\bar{G}_k^* = G_k \, exp(k_1 \, q^*)$$

$$\bar{\eta}_k^* = \eta_k \, exp(k_2 \, q^*)$$

$$q^* = \frac{q}{1 - d_t}$$

q^*: Mises stress undamaged
q : Mises stress damaged

Transient creep
(Kelvin-Voigt model)

Parameters: G_k, k_1, η_k and k_2
(Heussermann *et al.* 2003)

Steady-state creep
(Norton law)

Parameters: A_N and n_N

Tertiary creep
(Hou *et al.* 2003)

$$\dot{d}_t = A_T \frac{\left\langle \frac{f_{ds}}{\sigma_{ref}} \right\rangle^{n_T}}{(1 - d_t)^{n_T}}$$

Parameters: A_T and n_T

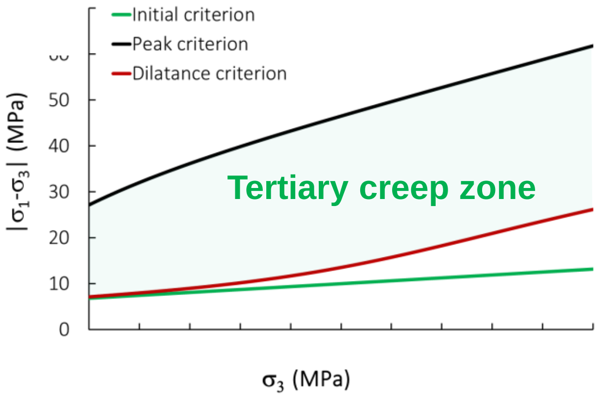

➔Damage is activated and increases if the damage limit (dilatance criterion) is exceeded

Numerical uniaxial creep test

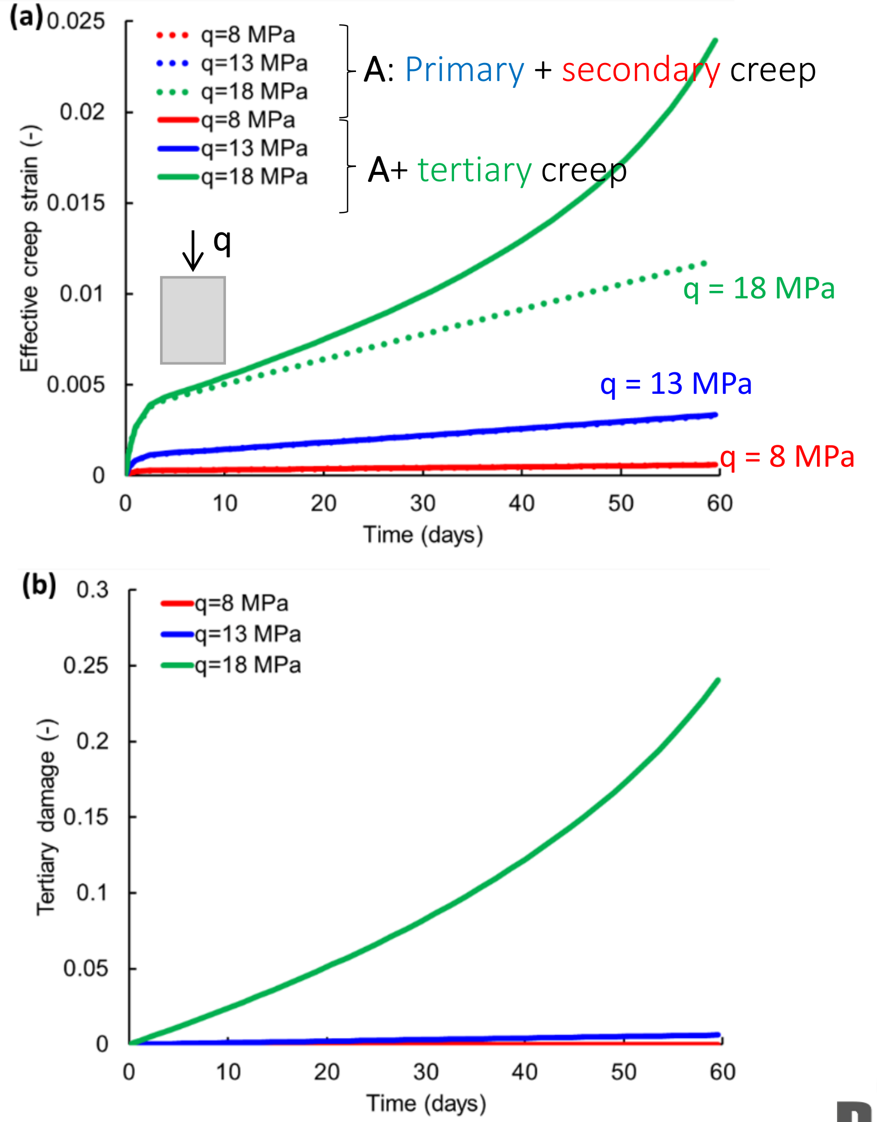

Proposed elastoplastic damage model

Full model equations (compressive stresses are negative and $\sigma_1 \leq \sigma_2 \leq \sigma_3$)

Damage:

$$f_d = d_{max}\{1 - \exp(-b_d(Y_d - Y_0))\} - d \leq 0$$

$Y_d = \sqrt{\langle \boldsymbol{\varepsilon} \rangle : \langle \boldsymbol{\varepsilon} \rangle}$ (Mazars 1984)

Y_0 = value of Y_d at $\beta(\gamma_p^*)$=0 ➔ f_{ds}

$d_{max} = d_{max}^0 \exp(a_d \sigma_3)$

a_d: parameter describing the effect of confining stress

d_{max} decreases from its maximum value due to confinement effect

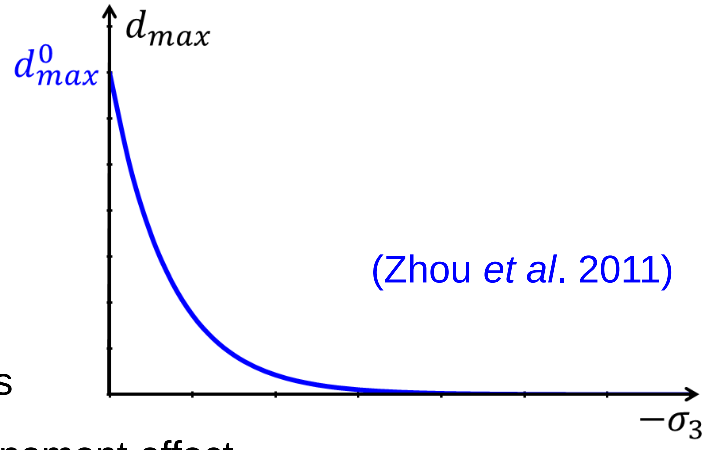

Dilatance criterion

$$\beta(\gamma_p^*) = 0;\ \gamma_p^* = -\frac{1}{b_\beta} ln\left(\frac{\beta_m}{\beta_m - \beta_0}\right) \qquad \Rightarrow \eta^p(\gamma_p^*)$$

$$f_{ds} = q + pM_{ds} - N_{ds}$$

$$M_{ds} = \eta^p(\gamma_p^*)\frac{\sin\phi}{\left(\frac{\cos\theta}{\sqrt{3}} - \frac{1}{3}\sin\theta\sin\phi\right)} \quad ; \quad N_{ds} = \eta^p(\gamma_p^*)\frac{c_i\cos\phi}{\left(\frac{\cos\theta}{\sqrt{3}} - \frac{1}{3}\sin\theta\sin\phi\right)}$$

Parameters:

E, ν

$c_i, \phi, \eta_o^p, \alpha^p, \beta_0, \beta_{m0}, b_\beta, d_{max}^0, b_d, a_d$

Hardening Plastic potential Damage

Thorel 1994 : $c_i, \phi, d_{max}^0, b_d, a_d$

Dragan *et al*. 2021: $E, \nu, \beta_0, \beta_{m0}, b_\beta$

geo Ressources

Numerical verification of triaxial tests

Short-term parameters values used

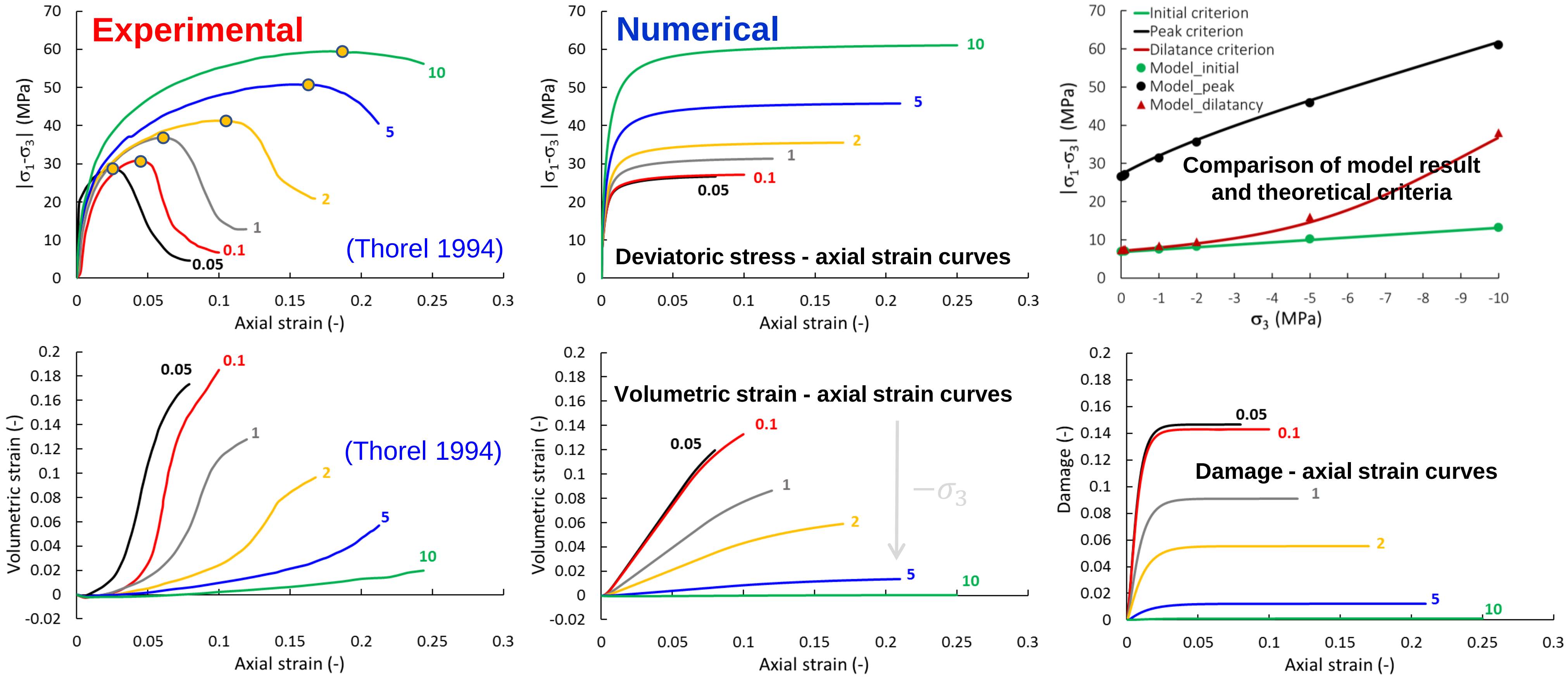

geoRessources